LANDSLIDE AGES AND IMPLICATIONS FOR A MARINE TERRACE AT RIALTO BEACH, WA

Chelsea Bush

A report prepared in partial fulfillment of the
degree of

Masters of Science
Applied Geosciences: Earth and Space Sciences

University of Washington

March 2020

Project Mentors:
Kathy Troost, University of Washington
Ian Miller, Sea Grant

Reading committee:
Kathy Troost
Alison Duvall

MESSAGE technical report number: 081

Acknowledgements

This project was encouraged and advised by Dr. Kathy Troost, who supported me both in the field and in the office, and helped me to make connections about this dynamic study area. Her mentorship has no doubt made me a stronger geologist.

Work in this region was inspired in part by Dr. Ian Miller, who initially questioned the origin of the marine terrace and remained a great source of insight and ideas throughout the process of this study.

As the second reader in my committee, Dr. Alison Duvall was a resource for important research in the study area, and gave scholarly and insightful feedback. Her support has been integral to this project.

Project funding for radiocarbon sampling was provided in part by the North Pacific Coast Marine Resources Committee (NPC-MRC), who are dedicated to learning about the Pacific Coast region and sharing knowledge with their community. Thank you to Ms. Tammi Pakorny for her help in allocating funding and for inviting me to present at the annual MRC meeting.

Wood identification was provided by Dr. Ed Espinoza of the USFS Forensics Laboratory in Ashland, OR and Dr. Michael Weissman of the USFS Madison, WI. Their expertise in wood genus analysis and thoughtful explanation of processes used was extremely beneficial to this project. I greatly appreciate their time and interest in this research.

This project would have been immensely difficult without Ms. Jill Silver, who allowed myself and my peers to stay at her delightful family cabin near Rialto. She has been important to this work by helping in the field, and sharing insights, delicious meals and enthusiasm.

Finally, a very special thank you to my friends and peers who came out to the field, in various weather, to help collect data. Elizabeth Davis was integral in all aspects of this project by assisting in tree coring, helping survey the marine terrace, assisting in surveying the hillslope and by sharing ideas, interpretations and field notes. Mary Alice Benson has spent several weekends on the coast with me assessing landslide areas, coring trees and questioning shoreline dynamics, and her impeccable field notes have been extremely useful. Thank you to Jonathan Paris for finding game trails to get us up the hills and for being a master tree corer. And thank you Varqa Tavengar, Devin Maloney, Morgan Simon, Zach Yakush and MESSAGe cohort 7 for spending time at Rialto tromping around and getting dirty!

Abstract

Holocene landslides and marine terraces at Rialto Beach, on the Olympic coast of Washington state, may provide clues about the response of the Pacific coastline and adjacent hillslopes to Cascadia subduction zone (CSZ) earthquake activity. This study uses seven ^{14}C samples from four distinct locations within a low-elevation marine terrace at Rialto Beach, WA to date landslides and constrain age of formation of the terrace. Two distinct landslides have been explored in detail: landslide 1 that occurred 800 years calBP, and landslide 3, that occurred 150-300 years calBP. The causes and triggers of these slope failure events were explored with new detailed field mapping and timing constraints. Observed landslide evidence includes hillslope geomorphology, soil composition of hillslopes, low-elevation marine terrace composition, and presence of slickenside bedrock-colluvium contacts within a drainage system. On landslide 1 I found a buttress unconformity on the hillslope containing interglacial peat and organic soil layer dated >48-27.5 calka, causing extensive zones of perching water that increases pore pressure and lowers slope stability. These geological layers are assumed to span the Rialto hillslope region. Dendrochronology to determine the age of trees on landslide 1 suggests that this slope was partially denuded during an intense winter storm in 1921 AD, potentially causing slope instability. Landslide 3, 150-300 yrs calBP sits atop the potentially uplifted marine terrace which contains beach deposits older than 500-600 years calBP. Dating suggests that the slide and uplift may be coseismic with the 1700 AD (270 BP) Cascadia subduction zone rupture. This study adds constraining dates of two distinct landslides that sit on top of the low elevation marine terrace, contributing to studies of coseismic uplift and landsliding on the Olympic coast.

Table of Contents

1. Introduction

The Olympic Peninsula of Washington State (Figure 1;2) has experienced tectonic deformation in the form of uplift, subsidence, and warping, as well as erosional modification from multiple alpine and continental glaciations, stream erosion and mass wasting, and sea-level fluctuations during the Pleistocene. These overlapping events create a complex geologic story, further complicated by the presence of dense forests along with their associated biological processes. Tectonics play an integral role in the formation and deformation of the region, and an important structure that has shaped the entire west coast, and the Olympic Peninsula, is the Cascadia Subduction Zone (CSZ). The subduction of the Pacific plate under the North American Plate (Figure 3) causes large magnitude (M_9) earthquakes, coastal subsidence, and tsunamis (Atwater, 1987). The last large earthquake occurred in 1700 AD (Atwater, 1987; Satake, et al., 1996) and recurrence intervals are estimated at 300 to 500 years (Atwater, 1987; Goldfinger et al., 2012). Researchers are looking for geomorphic evidence of tectonic deformation along the Pacific Coast of Washington, on the Olympic Peninsula (Riedel et al., *in review*; Sherrod, written communication). This includes marine terraces, dateable landslides and areas inundated by past tsunamis (Wirth and Frankel, 2019). Other relevant research includes the study of ghost forests; regions, usually near the coast, that contain dead trees that represent relict forests that have been affected by tectonic events and land-level changes (Ault, 2014).

The purpose of my study is to use radiocarbon samples collected from landslide deposits and the underlying Quaternary beach deposits within a low-elevation marine terrace along the Rialto beach coastline (Figure 2) to date the timing of past landslide events and to study possible landslide triggers, including strong ground motion from past earthquakes, storms or high precipitation events, and hillslope stratigraphy. Dating landslide deposits that sit upon a marine terrace also places new constraints on the timing and formation of that geomorphic feature. This terrace may have been uplifted during the last CSZ earthquake of 1700 AD. If so, that would indicate uplift occurred along the Olympic Peninsula coastline as a result of a large subduction zone earthquake and it would be the first documented zone of coastal uplift related to the CSZ (Sherrod, pers. comm.). According to Sherrod (pers. comm.) evidence of uplift is present on the northwest coast of Washington. The new landslide chronologies and constraints on the timing of marine terrace formation described here are important for hazard planning and resilience for communities within the Cascadia subduction zone.

To date landslides proximal to or on top of the marine terrace and explore triggers and causes of slope failure in the area, I focused on the following:

1) Carbon dating of wood material found within Quaternary beach deposits and overlying landslide deposits.
2) Tree cores collected from Sitka spruce on the hillslope to determine the age of the undisturbed modern ground surface to determine minimum age of the last landslide event.

3) Landslide mapping through digital and field observation, including review of satellite and LiDAR imagery correlated with field survey methods to identify significant topographical variances within the landscape.
4) Field survey to create a topographic profile and cross section of the hillslope, showing geologic units of the area, to explore geologic contacts and landslide causes and triggers.
5) Detailed sketch of 100-m long exposure of the low-elevation marine terrace showing geologic units within the low-elevation marine terrace, to explore past depositional environments.

In 2017 and 2018, researchers launched an investigation into the origin of a low-elevation marine terrace (Kathy Troost, written communication), funded by the North Pacific Coast Marine Resources Committee (NPC-MRC). Troost and UW MESSAGe graduate students completed preliminary radiocarbon dating, wood sample collection for identification, and palynology. They found that the low-elevation marine terrace consists of landslide deposits resting upon older beach deposits. Palynology and wood identification results support the presence of multiple landslides (Troost, pers. comm.). My report builds upon their foundational work and adds to a growing body of work on marine terraces along the Olympic coast (Sherrod, pers. comm.; Miller, pers. comm.; Riedel, pers. comm.).

2. Background

2.1 Tectonic Setting

The Olympic Peninsula is part of the CSZ, where the Juan de Fuca plate subducts beneath the North American plate, generating large magnitude earthquakes and regions of high topography, including the Olympic mountains (Thackray, 1996). The CSZ stretches 1000 km from north of Vancouver Island to Mendocino, CA (Figure 3). The northern Cascadia megathrust is 240 km wide, and is a low angle thrust fault with a dip of 11°, that extends to 40 km depth (Ramos et al., 2019). The subducting oceanic slab is 8-10 million years in age, and has a warm subduction interface, with a shallow brittle-ductile transition at 250-450°C (Wirth et al., 2018). Subduction along the CSZ caused high magnitude earthquakes during the Holocene along the Washington coast, resulting in land movement. The estimated recurrence interval of CSZ earthquake events is approximately 300-500 years (Atwater, 1987; Goldfinger et al., 2012). Paleoearthquakes have been recorded in the Cascadia submarine canyon through the study of turbidite deposits, allowing for a consistent record that informs recurrence models (Goldfinger et al., 2012). The average rate of plate movement during the Quarternary is 3 to 4 cm/yr. As evidenced in other subduction zones, coseismic uplift and subsidence can happen as a result of large subduction zone tectonic activity. This usually occurs on a strip of land adjacent to a submarine zone of uplift (Atwater, 1986).

The most recent CSZ earthquake occured on January 26, 1700 AD and has been recorded in historical accounts of tsunamis in Japan (Satake et al., 1996). Native American stories from oral histories from California to British Columbia describe this large earthquake occuring on a

winter night. Tribal storytelling in the northern Olympic Peninsula include accounts of shaking and large waves (Ludwin et al., 2005). Based on geological studies and documented tsunami heights and times in Japan, it is thought that this event represents a complete rupture, created by either an M_9 event or a series of M_8 events (Satake et. al, 1996; Atwater, 2005). Corroborating evidence for this event has been found in recent geologic studies on the Pacific coast of the United States, based on dendochronology and radiocarbon dating as well as presence of turbidites off the coast, although no evidence has been previously published from areas north of the Quileute River (Figure 4) (Satake et. al, 1996; Goldfinger et al., 2012).

Computer-generated models of megathrust events on the CSZ simulate varied responses to stress accumulation and rupture (Ramos et al., 2019). Models are compared with locations of known coseismic vertical displacement or geologic evidence of earthquake activity (Wirth and Frankel, 2019). Differences in land level changes found in the geology of the coast may have occurred due to shorter-wave high dynanic stress-drop events occuring along strike (Wirth, 2018). Models of vertical displacement attriuted to CSZ activity are also informed by studies in other regions with similar subduction slab properties, including the 2010 M_w8.8 Maule, Chile and the 2011 M_w9.0 Tohaku, Japan events (Wirth and Frankel, 2019). Strong -motion recordings of these events provide insight for modeling geological responses to CSZ earthquakes. Most models show subsidence along the coast, however, some modelling of CSZ events shows the possibility for uplift in the Rialto Beach area. Viscoelastic models using geodedic data show stress relaxation of locked zones through crustal deformation during interseismic periods occuring far from the fault. These models best match areas in later stages of seismic locking, such as present Cascadia. (Li et al., 2018).

2.2 Geologic and Geomorphic Setting

Two dominant geologic units make up the Olympic Peninsula: the oceanic basalt of the Crescent formation (Brown et al., 1960 taken from Tabor and Cady, 1978) and fossiliferous marine sediments, including shales, sandstones and volcanics, of Eocene, Miocene and early Pliocene age, known as the Hoh formation (Tabor and Cady, 1978). These marine sediments are faulted and folded, sometimes in stratigraphic order, although in areas of extensive deformation marine sediments make up a mélange and are brecciated. Deformation indicates east to west compression with overturned beds consistent with models of accretionary wedges in subduction zones (Tabor and Cady, 1978). Resistant sea stacks along the coast are composed of the Hoh formation mélange, including James Island to the south of Rialto Beach (Figure 2.B). This sedimentary sequence continues below the discharging Quileute River and under the beach and hillsides within the study area, outcropping along roads and within ravines.

The Olympic Peninsula has experienced both alpine and continental glaciation and contains glacial sediments from several advances during the Wisconsin glaciation and several preceding glaciations (Figure 5). On the Olympic Peninsula glacial and interglacial sequences are found, and multiple unconformities mean that younger glacial deposits can be sitting on much older interglacial deposits. South of the study area, at Kalaloch, silt/peat/gravel sequences

have been dated to deposition during MIS 3 and MIS 4 (Thackray, 1996). Due to maritime conditions in the area, which tempered the effects of global temperature changes, wood and vegetation debris are found in both glacial and interglacial deposits.

The Olympic Peninsula covers approximately 8,000 km, 80% of which is mountainous. The highest of these steep ridges is Mount Olympus, standing at 2,431 meters above mean sea level. The mountain range is oriented northwest to southeast, rising from sea level at Cape Flattery at the northwest point of the state, reaching a maximum height at 40 km along the range at Mount Olympus, and dropping to sea level again at Hood Canal at a total of 53 km (Danner, 1955) (Figure 6). The coastal portion of the Olympic National Park includes a 64-kilometer stretch of uninhabited beaches with variable character; some dotted with resistant sea stacks, some with undulating bluffs, still others with steep forested hillsides and towering trees (Figure 6). Highway 101 is the only main thoroughfare in the region, with few local roads allowing access to park visitors, locals, and members of the Hoh and Quileute Tribes (Geology of National Parks, 1955).

2.3 Climate and Coastal Environment

The Olympic Peninsula has a maritime climate, with an average rainfall range of 178-254 cm on the coast (Spicer, 1986). Vegetation in the region reflects the high levels of precipitation, with dense wooded zones of large, water-loving plants and temperate rainforests. Mid-latitude cyclones affect the Pacific coast of the Olympic Peninsula, creating winds comparable in force to Category 2 and 3 hurricanes, with wind speeds of 110-210 kmph. Effects of these storms includes damage to heavily forested areas along the coast. Strong winds from major storm events are associated with 80% of tree death in the Pacific Northwest (Kirk and Franklin, 1992). High levels of precipitation in Autumn combined with steep terrain cause saturated soils to lose adhesive properties, leaving root structures susceptible to windfall during high wind events. Wind speed gradients are enhanced in the Pacific Northwest's high-relief terrain, and areas with topographic barriers create elevated regions of ageostrophic flow that compounds wind damage (Mass and Dotson, 2010). One significant storm event that affected the study area and much of the Olympic coast is the "Great Olympic Blowdown" of 1921 (Figure 7). This storm caused loss of 40% of trees over the southwest portion of the Olympic range and 20% of loss along the Olympic coast (Mass and Dotson 2010, from Day, 1921).

The Olympic Peninsula coast is a high-energy storm-wave environment, with the highest waves occurring in December at an average of 4.3 m, and the lowest in August with an average of 1.5 m. Olympic coast tides are mixed semi-diurnal and meso-tidal (McKay and Terich, 1992). Rialto Beach is a fringing barrier with a barrier spit jutting out north of the Quileute River, connecting James Island to the coast (Figure 3b). Changes to this spit resulted from coastline retreat during Holocene sea-level rise, leaving behind the resistant conglomerate rocks of the Hoh formation that still exist as James and Little James Island (McKay and Terich, 1992). Seasonal changes to the beach profiles show asymmetry, suggesting barrier instability and overwash (McKay and Terich, 1992). Backbarrier slopes are lower than foreshore slopes. Dynamic beach cusps indicate a reflective beach environment (McKay and Terich, 1992). Seasonal overwash indicates that the barrier is moving landward, also evidenced by trees affected by salt spray and beach sediment within the forests proximal to the shoreline.

2.4 Rialto Beach Study Site

Rialto Beach, located on the Olympic National Park coastal strip, is a flat sand and gravel beach with coastal forest uplands (Figure 2). The beach spans approximately 2.5 km, from the parking area off of Mora Road on the south end to the beach terminus known as the Hole-in-the-Wall, a popular tourist backpacking destination (Figure 2.B). A sea stack comprised of the Hoh formation mélange called James island sits south of Rialto Beach, and a riprap structure connects it to the mainland and separates the Rialto area from La Push beach to the south, which is Quileute tribal land. Large driftwood logs make up the back berm, which can top 3 m in height and move throughout the year through wave and storm activity, emphasizing the dynamic nature of the beach area. Beach sediment is composed of flat gravel to cobbles of predominantly greywacke, that also move and create berm structures seasonally and during coastal storms.

Rialto beach contains wooded hillslopes covered in Sitka spruce and patches of alder abutting 2.5 km of coastline. Rialto Beach vegetation includes forests of Sitka spruce, a hearty, fast-growing conifer more resistant to salt spray that other regional trees like western hemlock, western red cedar, and Douglas fir that are found farther inland. Dense understories of salaal, fern and salmonberry cover the hillslopes adjacent to the beach, with poorly-drained areas showing expanses of skunk cabbage and horsetail.

The Quileute River discharges just south of Rialto Beach (Figure 3.A). Although the river once deposited glacially-derived sediments with provenance from both the Cordilleran glacial sheet and Olympic alpine glaciations, the source from these deposits has dissipated and the beach barrier is retreating (McKay and Terich, 1992). The river has shifted over time, though early accounts put the mouth of the river just south of James Island, near its current position, in 1889 (Reagan, 1909). Since 1953 multiple efforts have been undertaken by the Army Corps of Engineers to maintain the barrier spit to protect the boat harbor to the south, including the construction of dikes, rip-rap, bulkheads and sediment fills (U.S. Army Corps of Engineers, 1974 from McKay and Terich, 1992).

The study area consists of a dissected slope with multiple landslides, a low-elevation marine terrace, a back-beach wetland, and an active beach. Multiple drainages run perpendicular to the coast from near the top of the slopes, discharging in wetland areas at sea level. Ellen Creek is a significant drainage that dumps into the ocean and includes wood debris at the mouth (Figure 8). The hillslopes average 200 m in elevation, with hummocky landscapes.

A marine terrace parallels the coastline, from the parking lot north to Ellen Creek (Reidel et al., *in review*). Terrace height is 1-4 m, with higher elevation toward the north. The terrace contains Quaternary beach deposits topped by landslide deposits. Quaternary beach deposits are distinguished by oxidation, higher density and higher elevation than modern beach. The face of the terrace is exposed by wave erosion and exposure of the marine terrace changes seasonally and during storms. Beach grasses and trees grow atop the terrace. The terrace and other geomorphic features indicative of uplift have been hypothesized to result from CSZ megathrust earthquakes (Sherrod, pers. comm.). In general, marine terraces are formed by the rise and fall of sea level over time coupled with tectonic uplift. As sea level rises, erosive wave processes cut higher onto the shoreline. Tectonic activity, either sudden or gradual, uplifts the terrace above the influence of these wave processes, preserving the terrace (Figure 9). Thus paleomarine

terraces contain layers of beach sediment similar to modern beach deposits, including storm berms and high and low tide marks (Schulz et al., 2018).

Rates of vertical land movement (VLM) vary along the Washington coast, with noted regions of subsidence proximal to areas of observed uplift, both along the shore and inland. This shows complicated patterns of deformation and shoreline movement. Near the study area slow subsidence (0.5mm-1.5mm/yr) is occurring (Figure 10). (Miller et al., 2018). Subsidence and uplift measurements were obtained by assimilating multiple data types and methods to create a comprehensive analysis of elevation changes on the Washington coast. The three methods used include continuous GPS, tide gauge differencing and survey marker leveling from multiple locations (Miller et al., 2018).

3. Methods

3.1 Field-Based Cross Section

To constrain the origin and age of the low-elevation marine terrace, several methods were employed, including identifying landslides on LiDAR that provide minimum timing constraints on the terrace. Landslides that were further investigated in the field are labeled LS1 through LS4 (Figure 8). At the time of my study, LiDAR of the region was of poor quality, leading to field mapping techniques to capture the topographical relief of landslide 1 (LS1).

A field-based geologic cross section was completed from the beach at radiocarbon site 1 to the top of the hillslope, roughly perpendicular to the shoreline. Horizontal distance between two points at eyeline was measured using a tape measure, along with the angle measurement of the hillslope, using a hand level. The tape measure was then moved to the last measured point, and the next feature of interest along the transect, and new distance and angle measurements were recorded. Vertical height and horizontal length at each point were calculated using trigonometry (Figure 11). Vertical height and horizontal distance were added for each new transect location and plotted in Microsoft Excel. Hillslope and drainage geomorphology, geology, vegetation and potential landslide features were described along the transect. The ground surface profile was also supplemented with geologic information obtained by mapping outcrops in the gullies on the north and south side of LS1 (Figure 8).

3.2 Tree coring

The initial purpose for coring trees on LS1 was to determine age of deformation related to landsliding to further constrain landslide ages. It became obvious that this process was not feasible due to the naturally-occurring curved trunks of the trees, particularly those growing on nurse logs. Tree ages were collected to determine the age of the living forest and modern ground surface to calculate a growth curve relating tree age and diameter. Growth variables, including sunlight availability, whether the tree was growing on a nurse log, and tree location (top, middle or low bench), were also recorded for further analysis.

Haglof Increment borers (18”, 24”, 32” and 39” borer length) were used to collect tree cores from Sitka spruce along the hillslope with the intention of determining tree age and age of

tree deformation to aid in dating landslides. Trees were selected to get a representative sampling of varied tree diameter, as well as elevation on the hillslope, in hopes of determining a growth curve relationship between tree diameter and tree age.

The following steps were employed, following guidelines of Speer, 2010. Tree core field methods included measuring tree diameter with a tree diameter tape at mid-chest height, and recording height of core from the ground surface. A compass bearing was taken for each core direction and recorded. The outer bark of the Sitka spruce was removed with a chisel to expose a fresh surface. Then the increment borer bit was pushed into the trunk, holding the shaft level, and the handle turned clockwise until the shaft advanced past the center of the tree (Figure 12.A). To remove the core, a metal spoon was pushed into the core barrel into the center of the borer handle and the handle was turned counter-clockwise two times to release the core from the borer. The spoon was then removed, revealing the tree core. Two cores were collected from each sampled tree, roughly perpendicular to one another. To store the tree cores in the field, plastic tubes were labelled with sample ID, compass direction of core, date and bark side of the tree and cores were placed inside and ends capped. Small holes were poked in the plastic tubing to reduce moisture that leads to core molding.

To prepare the tree cores for accurate age counts, cores were mounted on wooden core mounts that were routed with a circular groove to hold cores in place for subsequent sanding. Cores were mounted with cross-sectional view up to ensure that ring boundaries were evident under the microscope, then ores were glued and wrapped with string to keep them straight while drying (Figure 12.B). Once dry, core surfaces were sanded using a belt sander and epoxy was applied to the surface. Tree core age data was determined by counting ring boundaries under a microscope. Two tree core counts for each of the sampled trees were averaged to determine the tree age.

Twenty-four trees were cored, and nineteen successful tree core sets were collected. Tree age and diameter were graphed in Excel to determine any relationships between age and size. Trees were also compared based on the following variables: sunlight availability and if the tree was growing from a nurse log, and combinations of these variables. Tree location relative to the three noted hillslope benches was also used to determine growth variability based on proximity to salt spray near the low bench proximal to the beach. Linear equations and R^2 values were calculated in Excel.

3.3 Terrace Mapping

The low-elevation marine terrace was evaluated in the field by surveying and mapping a 100-m length of the face, evaluating strata within, and compiling radiocarbon dating from the underlying beach deposit and mapping overlying landslide deposits. The 100-m long survey of the marine terrace was completed by collecting elevations of exposed units within the terrace using an auto level and stadia rod. A 100-meter measuring tape was stretched along the modern beach below the terrace feature, and the auto level was set up at a high point atop the terrace. Elevations were read and recorded along the transect at 2-meter intervals travelling north along the stretched tape. Elevations of unit contacts were also read and recorded at these intervals. The survey includes radiocarbon site 3, which was well exposed during the time of survey. Seven distinct units (A-G) were described on the basis of grain size, color, relative density, presence of

bedding features, presence of organics, presence and type of lithics, and type of contact. Features such as slumping by overlying units and cover by modern beach deposits were also noted.

3.4 Radiocarbon Dating

To constrain ages of deposits in the study area, wood, charcoal and organic soils were collected for radiocarbon dating at different elevations within the terrace; this included overlying landslide deposits and underlying quaternary beach deposits. A total of seven radiocarbon samples were collected for ^{14}C analyses from four distinct locations within the terrace feature that parallels the shoreline (Figure 8). Samples were collected in aluminum foil and placed in plastic Ziploc bags, labelled with Sample ID and date. GPS points were taken at all four locations.

In the lab, samples were rinsed with deionized water to remove sand and debris under a microscope and allowed to dry. Each dried sample was weighed to 30-50 mg of material and placed in a separate, labeled glass vial and plastic bag for submittal to National Oceanic Sciences Accelerated Mass Spectrometer (NOSAMS) Woods Hole Oceanographic Institute for analysis. A duplicate sample was sent to Direct AMS to determine feasibility of results. Results were reported in radiocarbon years ^{14}C BC. Dates were calibrated to calendar years using Oxcal v.4.3 (Bronk Ramsey 1995, 2009, and 2017) using the IntCal13 calibration curve (Reimer et al., 2013).

3.5 Wood Identification

Fragments of wood and trees were found in landslide deposits. Wood identification was performed using two processes: visual inspection through thin section at the USFS Wisconsin Lab by Michael Weissman, and ICPMS chemical processes by Ed Espinoza at the USFS Forensic Laboratory. This was performed on wood collected at radiocarbon site 1 and on wood from the ravine on the south side of LS1, in order to determine wood genus of the radiocarbon dated wood samples.

Forensics lab methods include submitting samples to test for phytoelexins, chemically diverse substances produced through plant tissue to fight parasite growth, growth hormones that contribute to pollen creation. The database that the samples were tested against currently contains 1500 molecules against which the samples were tested (Ed Espinoza, pers. comm.).

Visual identification methods include macro and microscopic observation, and sample preparation to clean out decayed and discolored regions. Modern wood ID relies on odor and color, which were not useful for this long-buried deposit. Wood-growth features distinctive to specific genus, such as nodular end walls and indentures, ray thraechids and ray parenchyma, can become filled with resin over time, making identification difficult (Michael Weissman, pers. comm.). Samples were boiled to drive out air and to make cleaner thin sections for identification through the microscope.

Another aspect of ongoing research in the study area is palynology research to determine past ecological environments.

4. Findings

4.1 Marine Terrace

4.1.1 Description of Terrace

The low-elevation marine terrace stands 1 to 4 meters high, and is highest near the most recent landslide area (LS3 on Figure 1). The top of the terrace is covered by grasses with standing Sitka spruce, some of which are dying. Between the terrace feature and the hillslopes is a wetland area with skunk cabbage, fern, and horse tail. This area contains ponded water in some lower-lying areas. The terrace contains downed wood from upslope as well as driftwood pieces moved by wave action. The terrace has been breached at several locations where gullies drain water from the slope. The terrace face and exposure of units within the terrace changed with each field visit, as modern beach gravel and wood was accreted or eroded from the terrace. The terrace surface consists of a veneer of modern beach gravel or silty colluvium (landslide deposits with angular bedrock clasts).

4.1.2 Radiocarbon Dating

Radiocarbon samples collected from four sites show varied ranges after calibration (Table 1; Figure 13). Each sample age range shown is within one sigma range (95.4% probability) based on OxCal calibration to radiocarbon years calBP (Appendix 2).

Sample site 1 shows landslide deposits with wood overlying oxidized sand and gravel layers inferred to be old beach deposits. Wood pieces from within the landslide at sample site 1 (Figure 8; Figure 14A), sample MAB 24-18, shows an age range of 694-793 years calBP. This area of terrace was completely covered by a veneer of modern beach in July 2019 (Figure 14B).

Three radiocarbon samples were collected from sample site 2 (Figure 8; Figure 15). MAB 25-18 S1 is a wood sample collected 72 cm from the top of the marine terrace with a range of 514-630 yrs calBP and MAB 25-18 S2 is a charcoal sample taken 54 cm from the top of the marine terrace with a range of 506-539 yrs calBP. These samples are from old beach deposits. MAB 24-18 S5, an organic soil with ribbons of peat, with dates ranging from 2469-2847 yrs calBP, is the oldest tested sample from the terrace.

The two youngest samples were collected from sample site 3 (Figure 8; Figure 16), with KT 32-18 S1 collected 65 cm below the top of terrace within a layer of silt and gravel with bedrock clasts (landslide deposits), showing results of a date range of 2-304 yrs calBP. KT 32-18 S2, collected from 10 cm below top of terrace within the same landslide deposit, has a date range of 14-290 yrs calBP. These samples were collected from a dynamic portion of the marine terrace where a landslide toe is being eroded (Figure 17).

At sample site 4, sample KT 200-18 S1 was collected from the left bank of Ellen Creek within an old beach deposit (Figure8; Figure 18). Results show a date range of 563-668 yrs calBP. The ages correlate with old beach deposits collected from sample site 2, as indicated in Figure 12 by the light grey bar showing similar radiocarbon ages. A duplicate sample of KT 200-18 S1 was submitted to Direct AMS for confirmation of data, with lab results showing an age range of 514-630 yrs calBP (Table 1).

4.1.3 Terrace Composition and Mapping

A 100-meter-long survey of the exposed marine terrace shows elevations of unit contacts and includes radiocarbon sample location 3 (Figure 8). The terrace contains multiple diamict layers with woody debris (units A, B and D), a clean sand layer with organics (unit C) and a massive clay layer with organics (unit G). The top two units are diamicts that coarsen upward, with a variability in the angularity of bedrock clasts (units E and F). Most of these units are horizontally continuous with variable thicknesses, showing the dynamic depositional and erosional environment of the coastline. The face of the terrace is oriented at330º. The geologic cross section (Figure 20) is shown as a series of panels (Figures 21 through 25) at a larger scale for viewing. Seven distinct unit descriptions and their extents follow:

Unit A-

Stiff dark brown to brown clayey SILT with cobbles and pebbles in lower 1-1.5 m portion. With organics including pieces of bark, twigs, sticks, cones and needles adhered in sheets. Undulating contact with oxidized sand and gravel of unit B. Horizontal ribbons of oxidation.

Unit A extends from 0-9 m on the survey. Unit A has uneven, lobate features. The unit thickness ranges from 0.2-0.8 meters at 5.2-9.0 m along the survey (Figure 25).

Unit B-

Very dense, dark to medium brown SAND with flat oval-shaped gravel and cobbles with lenses of coarser sediment. Mostly quartz. Occasional imbrication. Varied lithology, including greywacke and some granodiorite.

Unit B extends from along horizontal distance 5.2-9.0 m before pinching out, and then is exposed from 10.0 -17.0 m with higher concentration of cobbles towards the top of the unit. The unit is covered by modern beach deposit at the bottom contact, with a flat contact with unit C above from 14.0-17.0 m (Figure 25). From 60.0-67.0 m unit B is exposed with an undulatory contact with unit G above. Unit thickness ranges from 0.2 meters at 60.0-63.0 meters, where a slump of unit F covers unit B, and grades to a larger exposure thickness of 0.6-0.8 meters at 63.8-66.4 meters, with more cobbles exposed in the lower portion of the unit (Figure 22). Modern beach deposit covers the unit until 75.0 m, where unit B is exposed with a thickness of 0.4 m and elevation of 2.0-2.4 m, and has a relatively flat contact with unit F above. From 82.0-96.0 m unit B is exposed with a maximum thickness of 1.3 m, ranging from 0.80-2.29 m height. Modern beach cover from 80.0-84.0 m and 94-100 m creates a lens shaped unit exposure. Unit B is cobble supported from 84.0-86.0 m at elevation 0.80-2.25 m. The unit has a contact with unit G from 85.0-90.0 m, with logs located at 87.0 m and 90.0 m at the contact. The unit has a straight contact with unit E from 91.0-100 meters (end of transect). The unit is chaotic, with random cobbles and sand lenses, from 86.0-90.0 m and elevations of 0.69-2.49 m. From 96.0-100.0 m the unit has sand lenses at elevation of 0.79-0.99 m (Figure 21).

Unit C-

Dense, golden-tan fine to medium SAND with gravel. Well-sorted, sub-rounded, clean. Predominantly quartz with garnet, epidote and magnetite. With organics including decaying roots and 2-10mm charcoal pieces.

Unit C is exposed under unit D with a sharp contact in three distinct areas of the survey. The unit is laterally extensive along the survey but at times obscured by modern beach deposits. First exposure is at 14.0-17.0 m and 2.0 m elevation above unit B and below unit D as a clean sand with sub-rounded gravel, with modern beach deposit covering all units from 17.0-20.0 m (Figure 25). From 24.1-28.5 m at elevation 1.79-2.19 m, charcoal pieces 2-10 mm in size are exposed within the upper part of unit C overlying fire cracked rock (Figure 24). This exposure creates a clear contact with unit D above and with modern beach deposit below. Unit C outcrops again from 33.0-36.0 m as a clean sand with organics, exposed from 1.10-2.30 meters elevation with a clear contact under unit D (Figure 24).

Unit D-

Dense, dark brown to brown SAND with gravel. Coarser, pebble-and-cobble-supported material in lower 0.3 m of unit. Undulating contact grades over 4 cm and does not follow topography.

The first exposure of unit D is from 15.0-17.0 m at an elevation of 1.20-2.19 m, in contact with unit C below and unit E above. Modern beach covers all layers from 17.0-20.0 m. Unit D extends from 20.0-36.0 m with elevations of 2.19-2.69 m, and layer thickness ranges from 0.2-0.8 m. The unit shares a bottom contact with unit C and an undulatory top contact with unit E (Figure 24).

Unit E-

Medium density, golden-brown SILT with sand. With angular bedrock clasts, organics, charcoal and wood fragments. Dry.

Unit E is first exposed from 15.0-17.0 meters at elevation of 2.49-2.70 m. Unit E is then exposed from 20.0-37.6 m at elevations ranging from 2.19-4.79 meters, and has a bottom contact with unit D. Unit E is the uppermost unit in this portion of the terrace. Scattered wood debris and charcoal are concentrated within the lower 0.3 m of the unit (Figure 24) with a large tree root at 35.0 m. Modern beach deposit obscures unit E from 37.6-48.6 meters. Unit E is exposed again from 48.6-60.0 m at elevation of 1.90-2.49 m, with areas of concentrated angular lithics from 55.0-57.0 meters and 58.2-59.6 meters, and a thickness of approximately 0.3 m. This exposure has a coarsening upward sequence, and has a flat contact with unit G below and an undulatory contact with unit F above (Figure 23).

Unit F-

Medium density, greyish brown SILT with sand and highly angular clasts of weathered bedrock (sandstone) of variable size (2-12 cm). Dry.

Unit F is first exposed at 37.0 m and extends the rest of the survey going north. The elevation range is from 1.89-4.89 meters, with greatest unit thickness of 2.6 meters at a horizontal distance of 50.0-60.0 m (Figure 23). A slump of unit F from 61.8-65.0 m covers units G and B below, reaching modern beach deposits (Figure 22). Unit F shares a contact with unit E from 48.6-60.0 m and 93.0-100.0 m. Unit E shares a bottom contact with unit G from 60.0-66.4 m and 85.0-90.0 m, and shares a bottom contact with unit B from 75.0-85.0 m and again from 89.0-91.6 m (Figure 21). This unit is the uppermost unit on the survey where it is exposed.

Unit G-

Medium density grey silty plastic CLAY with 2-10mm charcoal fragments. Moist. Bands of oxidation on unit face. Discontinuous.

Unit G outcrops at 50.0-66.4 m, at elevation of 1.60-1.80 m, with a sharp undulating contact with unit B below and flat contact with unit F above. The unit increases in thickness going north along the survey (Figures 22 and 23). There is an increase in oxidation and organic content exposed on the terrace face at 54 m. Unit G has slumped and broken onto the modern beach deposit at 59.0-67.0 m. A second exposure from 84.8-90.0 m and elevation 2.1-2.5 m contains large pieces of wood near the base of the unit (Figure 21).

4.1.4 Erosion and Burial

The low-elevation marine terrace has experienced erosive processes and intermittent burial of the terrace throughout the time of my study. The locations of radiocarbon samples 1 and 2 were terrace exposures in June, 2018, when radiocarbon samples were collected, with an approximate height of 1-2 m (Figure 8; Figure 17A and B). At the time of sample collection, the terrace exposure at radiocarbon sample site 3 was approximately 2 meters in height and exposure included unit F, with modern beach deposit obscuring lower units (Figure 17C). At the time of the construction of the marine terrace survey, an additional 1.5-2.0 m of the terrace was exposed at this location, along with new unit exposures: units A, B, C, D, and G were visible within the terrace near sample site 3 starting in July of 2019, and those exposures became larger as the terrace material was removed by wave action and storm events during the months between July and October 2019 (Figures 17B and 17C). In particular, more of unit G was exposed by ¾ meter (Figure 26).

Radiocarbon sample site 1 was completely covered by modern beach in July 2019 (Figure 14B). Sample site 2 was covered by modern beach deposits in July, 2019 (Figure 15B). Between June 2018 and October 2019, the terrace at sample site 3 showed more than a meter of new vertical exposure of old beach deposit (Figure 17). Wave action caused sloughing of the terrace and a large Sitka spruce growing on the top of the terrace fell onto the beach below.

4.2 Upland Slopes and Landslides

4.2.1 Landslide Mapping

LiDAR imagery and field investigation show areas of potential landslide features on the Rialto coast in the forested uplands proximal to the beach (Figure 8). LS1 is an area with an arcuate headscarp and three nested bench features below (Figure 27). This landslide feature is bounded to the north and south by drainages with running water. Vegetation in the area includes large stands of Sitka Spruce and regions of dense salaal, salmonberry and fern. Just upland of the beach wetland depressions contains plants such as skunk cabbage and horse tail. Within the hillslope, hummocky terrain dominates, with fallen and rotting trees mostly oriented roughly north-south on steeper portions of the hillside. The area is overgrown and soil exposure is largely found near the drainages or within large rootwads. LiDAR imagery and field observation suggests rotational slide events. Landslides include evidence of landslide deposits on and in the marine terrace, with bedrock clasts strewn about the top of the terrace, indicating the landslide toes may have reached the ocean.

Radiocarbon site 2 LiDAR shows an arcuate headscarp and amphitheater bowl-shaped feature below (Figure 8), and field observation from the beach shows the area filled with alders and salaal. This area was too densely forested to field check, but the LiDAR shows a scarp feature near the top of the hill with hummocky terrain below, and definitive headscarp boundaries to the north and south near active drainages. This suggests a deep-seated rotational slide.

Radiocarbon site 3 shows an arcuate headscarp feature and hummocky terrain below (Figure 8). Field observation shows a patch of alder trees within the headscarp depression, and as alders tend to grow in recently disturbed soils this further indicates an area affected by slope instability. The area below this region was captured in the marine terrace survey, which has varying thicknesses of landslide debris in different stages, including initial runout of clayey silt, which may be the water-logged lighter particles (unit G) , followed by silty matrix with smaller bedrock clasts (unit E) and the bedrock clast supported, heavier colluvium deposit above (unit F).

4.2.2 Cross section of Hillslope

The field-based cross section (Figure 27) and mapping provided information on LS1 (Figure 1). This slope has one active drainage to the north and one to the south that define the width of the hillslope to be about 120 m. The cross section is 250 m in length and terminates on the top of the hillslope of LS1, with a relative direction of west to east. The topographical profile shows three bench features, with the top bench at an elevation of 76 m and cross section terminating at the bottom of the slope, at 2 m elevation (Figure 26).

The landslide contains three relatively flat benches, the top bench at 76 m in elevation, the middle bench at 55 m elevation, and the low bench at 32 m elevation. The upper slope is at roughly 42%, the middle slope is 33%, and the lower slope is at 74%. The benches range from 90-120 m in width, with the widest bench at the top, above where the constraining drainages begin on the hillslope. The top bench and low bench create depressions that are slightly back

tilted to the east, and create depressions that hold water and create wetland areas. The middle bench is flat. At the base of the hillslope, back side of the terrace, a wetland depression contains saturated soils and wetland index vegetation, including skunk cabbage, horse tail and fern. The ground elevation then slopes slightly upward from the edge of the wetland area towards the beach.

The hillside contains landslide deposits and colluvium over a glacial and interglacial deposit over bedrock (Figure 26). The LS1 landslide deposit consists of silt and sand with angular sandstone bedrock clasts. The glacial deposits contain rounded pebbles to cobbles in a sandy matrix. Interglacial deposits include dense organic silt and peat that make up the bottom of the southern drainage.

Till comprises the first bench. The till is a diamict with silty matrix and rounded gravel to cobble-sized lithics. Glacial till is also found within the hill slope, and exposed in root wads of fallen trees on the top bench (Figure 28). No glacial deposits were discovered below approximately 50 m in elevation. The interglacial deposits are peat and organic silt with a sulfur odor. The deposits are exposed within the southern gully of LS1 at 71 m elevation. At 67 m a gully within the southern ravine of LS1 contains a peat layer with lenses of sand and gravel, with peat dated 27.9-30.9 calka (Figure 29A; Table 1). A contact between the glacial and interglacial layers was found within this drainage at 63 m elevation. This interglacial layer extends west, creating a contact along the sandstone bedrock that is intermittently exposed along the southern drainage of LS1. The peat is saturated and of low permeability. This layer also has a ~10 m exposure in this same gully from approximately 20 m to 30 m elevation, with large pieces of wood that have been dated to >48 calka and identified as Sitka spruce (Ed Espinoza, USFS Forensics Laboratory, pers. comm.) (Figure 29B; Table 2).

At 8 m elevation within the northern ravine of LS1, a contact between colluvium and sandstone bedrock shows slickenside features (Figure 30). A relict channel to the north within the ravine is also present, with evidence of an abandoned knickpoint feature and debris associated with an old drainage. The knickpoint is derived from the more resistant sandstone bedrock of the Hoh formation. The modern drainage sits ~ 2 m to the south.

4.2.3 Tree Ages Based on Tree Cores

Nineteen living Sitka spruce were successfully cored. The trees had various diameters and positions on the hillslope of LS1 (Figure 31). Tree diameter vs. age of all data points show a linear regression line of $y=0.2043 + 58.545$ and an $R^2=0.3018$ (Figure 32; Table 3; Appendix 1). Diameter does not correlate well with tree age.

Cores collected from four trees growing on the ground surface with low sunlight availability show a linear regression of $y=0.154+67.222$ with $R^2=0.3512$ (Figure 33). Three of the trees located on the top bench are larger in diameter and higher in age but fall at or below the linear regression line, while the cored tree on the middle bench falls above the line. The tree located on the lower bench is on the linear regression line but youngest and smallest in diameter.

Tree cores collected from four trees growing on the ground surface with high sunlight availability show $R^2=0.7465$ (Table 3). Tree 16 is located on the top bench and has the smallest

diameter and age, while trees 11 and 17, located on the middle bench, fall above and below the linear regression, respectively (Figure 34; Appendix 1).

Core diameter vs. age data for five Sitka spruce growing on nurse logs with low sunlight availability show an R^2=0.6262 (Table 3). Core samples 18 and 19 show trees located on the middle bench that plot above and below the regression line, respectively (Figure 35). These are smaller in diameter and younger. Tree 4 is located on the middle bench and falls on the regression line. Tree 24 is the largest and oldest tree core collected, and falls below the regression line. Tree 7 is located on the lower bench and falls above the linear regression line (Figure 31; Appendix 1).

Core diameter vs. age for six trees growing on nurse logs with high sunlight availability show a low R^2 value of 0.061, and the lowest age range, of 4.5 years, and diameter range of 50.8 cm (Figure 36; Table 3).

Plotting tree diameter vs. age of cores taken from seven trees growing on the low bench, closest to the beach, yields R^2=0.0155 (Figure 37; Table 3).

On the top bench, trees growing on nurse logs with high sunlight availability span age and diameter, with trees 2 and 3 falling above the linear regression line. Trees 1, 8 and 7 plot on the line. Tree 19, growing on a nurse log with low sunlight, plots below the line (Figure 31, Appendix 1).

The plot of tree diameter vs. age of cores collected from seven trees near the middle bench of LS1 show R^2=0.5051 (Figure 38; Table 3). Trees 18 and 10, both growing on nurse logs with low sunlight, fall on the line of regression, along with tree 4, growing on a nurse log with high sunlight availability. Tree 12 and tree 11 plot above the line (Figure 31; Appendix 1).

Five trees cored on the top bench of LS1 and directly above, when plotted against averaged counted tree age, show a strong R^2=0.9918 (Figure 39; Table 3). Examining growth variables shows that tree samples growing on ground surface with low sunlight availability, tree 16, tree 14 tree 13 and tree 6, plot along the line of linear regression, while tree 15 plots just below the line (Figure 31; Appendix 1). The ground surface on the top bench has less nurse logs.

5. Discussion

The shape of the slope and deposits in the marine terrace show evidence of multiple landslides along the slope north of the parking lot at the Rialto Beach study area. The evidence consists of colluvium (landslide deposits) of different ages, bench features, exposure of a slickensides, and hummocky terrain.

Ages of deposits and rapid erosion suggest that the marine terrace was uplifted. Timing of uplift has an upper constraint of dated wood in landslide debris on top of the terrace and a lower constraint of dated organics in underlying Quaternary beach deposits. Modeling of CSZ earthquakes show that a complete rupture followed by high dynamic stress drop events could create uplift along the coast, with areas of deformation dependent on subevent location and magnitude (Wirth and Frankel, 2019). Based on geomorphic evidence, radiocarbon dating and review of CSZ rupture models, it is possible that this marine terrace was coseismically uplifted

during the 1700 AD Cascadia rupture, with landsliding occurring and depositing on top of the terrace.

5.1 Hillslope History

To study the geomorphology of the hillslopes of Rialto Beach, I focused on LS1 in the field to determine the geology and stratigraphy of the area. Based on observation and radiocarbon dating, which dates wood entrained in the landslide toe of LS1 to 694-793 years calBP and LS3 to 146-304 years calBP, it appears that multiple rotational landslides have occurred on the hillslopes, with the gullies often creating borders between distinct landslides. Both landslides have the character of deep rotational slides, including arcuate headscarps and hummocky terrain.

Based on the geology at LS1, an interglacial peat layer confines groundwater and could therefore increase the probability of slope failure. If a landslide occurred during the January 1700 AD (270 BP) Cascadia earthquake, the slopes would have been prime for landsliding, given the increased precipitation and groundwater levels of winter. Radiocarbon ages from landslide deposits within LS3, with a range of 146-304 years calBP, suggest the possibility of a slide coseismic with the 1700 Cascadia event.

LS1 is less than 800 yrs cal calBP based on the radiocarbon age of wood debris found within the landslide toe, and greater than 100 yrs (50 yrs BP), based on ages of Sitka spruce growing on the hillslope. Hummocky terrain, along with the arcuate headscarp feature shows evidence of a past rotational slide producing three distinct benches. These may indicate multiple nested slides, or one slide event. Pollen analyses on the landslide debris around the wood that was dated indicate that the slope above site 1 was disturbed and then revegetated (Troost, written comm.).

The area of LS1 after landsliding has since been overgrown by dense underbrush and a forest of Sitka spruce no older than 100 years. This suggests a slope failure including movement of fallen trees occurring at least a century ago. Lack of exposed soils on the hillside supports this suggestion. Within the northern drainage of LS1, the contact between bedrock and colluvium has slickensides and the overlying broken-up landslide debris has an undulatory contact. An abandoned knickpoint in the area of the slide may suggest that the landslide forced the drainage away from its original course. Standing water and/or saturated soil were noted on the flat area at the top of the slope, in the flat areas on benches, and in the gullies above perching layers. The perching areas, particularly the peat in the interglacial layer in the south gully, would increase pore pressure, increase load, and decrease strength. These conditions may have contributed to landslide susceptibility.

Based on LiDAR imagery, LS2 shows an arcuate scarp hillslope feature that may suggest another rotational slide event. This area was not checked in the field.

The hillslope of LS3 is a bowl-shaped feature with a large patch of alders that appear to be of the same size, surrounded on all sides by Sitka spruce. As alders grow in disturbed soils, their presence directly upslope of the landslide deposit supports the idea of a significant rotational slide event (Figure 39). Fewer Sitka spruce stand among the alders on LS3, suggesting that the spruce trees standing before the slide came down with the material. Some of these trees

have been entrained within landslide debris, while others may have been later removed by wave action. Thus the radiocarbon wood dated during a coseismic slide is likely to represent the age of the event, as many trees were likely felled and entrained in slide material.

5.2 Tree Ages

Tree diameter vs. age data shows despite tree diameter, the Sitka Spruce tree cores have ages with a range of 43 to 101.5 years. The high end of the range is about the age of the Olympic Blowdown of 1921. This could indicate that the storm removed the standing forest in the area, felling trees that became the nurselogs that dot the landscape today, and potentially causing landsliding. Nurselogs provide nutrients to growing forests, and may have contributed to area reforestation. Nurselog height in the area represents the approximate diameter of the fallen trees which may have been standing before the 1921 storm.

Existing standing dead trees at the top of the hillslope were measured to have a diameter of approximately of 188 to 264 cm, which could be from the same age of forest felled by the storm (Figure 40; Appendix 1). Cores could not be taken from the dead trees because of rotting wood, but larger tree diameter suggests these trees may have been older than the modern forest when they died, and the relatively similar sizes may suggest they died at around the same time. Without standing trees to keep the soil on the hillside in place, the shape of the hillside would have been susceptible to sliding or movement due to rainfall or harsh winter storms. Soil runout may have increased due to lack of root systems, or build-up of soil mass behind fallen trees may have significantly altered topography to create hummocks or bench features. It would be reasonable to expect this slope failure mechanism to occur as a result of strong windstorms.

Trees growing on nurse logs with high sunlight availability show lower age range with highest average diameter, suggesting that sunlight and nurse logs contribute to tree growth.

Fewer nurse logs on the ground surface of the top bench may be due to trees falling down the slope during storms and remaining on the lower benches, where trees could grow. Trees growing on the top bench have the highest R^2 value of 0.9918, perhaps as a result of lowered effects of growth variables such as nurse logs, salt spray from the ocean affecting lower benches, and a more even distribution of sunlight availability. Trees on the lower bench show a tendency to grow on nurse logs with higher sunlight availability, due to the sunlight exposure from the west and less dense canopy of surrounding trees.

The linear regression for all tree core data plotted together shows a weak R^2 value of 0.3018, suggesting that variables aside from tree age contribute to tree diameter of Sitka spruce in the area. Trees on the top bench tend to be older and larger, suggesting that protection from salt spray and ocean storms may be the most important factor in determining reasons for variability in tree growth rate. Trees on the middle and low bench show mixed results with no determining pattern regarding tree growth rate variables.

Tree identification from radiocarbon sample site 1 is a piece of Western red cedar which is usually found in colder environments and less amenable to salt spray. Western red cedar is not currently found in the study site, suggesting the area may have had different tree types 800 years ago when the tree died. It is plausible that the shoreline may have been farther away to reduce amount of salt spray affecting the hillslope. Because the radiocarbon sample was found entrained

within colluvium deposit, it could have died before the slide occurred and hence been reworked or the tree was redeposited from a much higher elevation in growth position.

5.3 Age and Impacts on Marine Terrace History

Radiocarbon ages of wood found within old beach deposits at radiocarbon sample sites 2 and 4 suggest ages of 500 and 600 years calBP. These are overtopped by a landslide deposit aged 150-300 years calBP at radiocarbon site 3. Between these deposits is a massive grey clay with silt with charcoal inclusions, the date of which may indicate the age of uplift of the marine terrace (Figure 39). If the grey clay layer is dated to around 300 years calBP, this could be permissive with the terrace uplifting during the Cascadia subduction zone quake of 1700 AD (270 BP), and the deposition of landslide debris as a coseismic landslide event (Figure 41). Vertical land movement for the study area shows the region is currently subsiding at a rate of 0.5-1.5 mm/year (Miller et al., 2018). This suggests that if the terrace was uplifted 300 years ago it would have been 150-375 mm higher than the current elevation, given a steady subsidence rate. Current subsidence in the area suggests the past seismologic event may have included uplift of the study area, in part based on the viscoelastic properties of subduction zone deformation, and the rebound of the area after a significant CSZ rupture.

Units found within the marine terrace show possible scenarios of past depositional environments now exposed by wave action along the coast. Terrace height increases going north along the beach, and seasonal changes to beach morphology result in varying degrees of modern beach deposits covering the terrace exposure.

Possible depositional environments were interpreted and are provided below for each of the units described during the terrace transect:

> Unit A. Based on the fine-grained matrix, abundance of wood and plant debris, and an undulatory basal contact, unit A is inferred to be a landslide runout deposit. It could also represent a paleo ground surface.
>
> Unit B. The sand and gravel matrix with cobble lenses of this unit suggest these are alluvial deposits from drainage outflows. The brown sand color may suggest provenance from the sandstone bedrock exposed in ravines on the hillslope. The variance in grain size and range, pulses of coarse grain sediment, and occasional imbrication may indicate fluctuations in creek discharge.
>
> Unit C. The clean sand and lateral expanse of this unit suggests an old beach deposit. From 24.0-82.6, a horizontal layer of charcoal pieces above a layer of fire-cracked rocks is exposed, which may represent a beach fire. From 35.0-37.0 meters unit C is clean, with no cobbles, and has ribbons of decayed organics that may represent old tree roots. Directly above this area within unit E is a large old tree stump. The clean sand of unit C may suggest the old beach experienced coseismic uplift or was deposited during higher sea level stand, when the water was higher and beach came farther towards the hillslope. Garnet, epidote and magnetite in the sand indicates provenance from a Cordilleran ice

sheet. The contact with unit D shows a change towards lower sea levels as unit D reflects upper beach deposits with cobble-supported sand.

Unit D. This old beach deposit may represent the upper beach area during lower sea stand. The dark brown sand with pebbles and rounded cobbles mimic the modern beach deposits, but are dense and of darker color, with oxidation on the unit face reflecting age and exposure to saltwater.

Units E and F represent landslide material upslope of radiocarbon sample site 3, with similar composition but distinct size and shape of lithic fragments. Both units are diamicts with a silt matrix and angular bedrock clasts from the Hoh formation sandstone, the bedrock of the surrounding hillslopes. Unit E consists predominantly of silt and smaller Hoh formation sandstone chunks and may be lighter slide debris from a slope failure above, with pockets of clast-supported material within the unit. Unit F contains larger chunks of bedrock and is more clast-supported than unit E. This unit also contains more entrained wood. Unit F may represent slide debris with larger and heavier chunks of bedrock that deposited after the initial lighter slide material.

Unit G is a silty clay with charcoal pieces. This massive unit contains no bedding and may have been deposited during seismic activity from an earthquake. The unit sits on top of old beach and below landslide deposits within the terrace. The age of this deposit may determine if this was coseismic with the January 26, 1700 AD earthquake. This could be the initial saturated phase of a landslide during a winter precipitation event.

Landslide deposits E-G from 17.0-100.0 meters along the transect may be from the same slide event, which incorporates radiocarbon sample site 3; sample KT 32-18 S1 (2-304 years calBP) and KT 32-18 S2 (14-209 years calBP) collected from Unit F (Figure 20, Table 1). Presence of dense understory and a modern alder forest suggests that the inferred slide near radiocarbon sample site 3 occurred within the last 150-300 years. Based on stratigraphic deposits exposed on the marine terrace and LiDAR imagery, these deposits could represent one large slide event triggered by saturated soils from upslope that caused debris flow in stages. This landslide material may have slid on top of beach deposits that were simultaneously experiencing uplift from the Cascadia subduction zone earthquake on January 26 1700 AD (Figure 41). Over time, wave action has exposed the contacts.

The modern beach is moving landward, burying portions of the terrace in the southern area of Rialto, near the parking lot, while wave action is exposing and removing parts of the terrace near radiocarbon sample site 3. Trees along the terrace are falling seaward as material is removed from below. This indicates changes in beach morphology that could ultimately remove the terrace structure.

6. Limitations

Radiocarbon sample dates reflect the time that the tree died, not necessarily when the wood was deposited. This gives an idea of the age of the deposit but it is possible that the wood samples were already downed plants that were then deposited through landsliding, for

radiocarbon sample sites 1 (sample MAB 24-18) and radiocarbon sample site 3 (samples KT-32-18 S1 and KT-32-18 S2). It is also possible that wood samples within the old beach deposits, from radiocarbon sample site 2 (samples MAB-25-18 S1, MAB-25-18 S2, and MAB-25-18 S5) and radiocarbon sample site 4 (KT-200-18 S1) were pieces of deceased trees or charcoal distributed through wave action and not fully representative of the age of deposit. When trying to correlate the specific Cascadia subduction zone event of 1700 it is important to note that the sample wood may not have died at the time of the event.

LiDAR imagery used in this project is from 2014 and not of the best quality. Although geomorphic features are visible, the resolution is limited because vertical accuracy is too low to run analyses for slope roughness/stability assessments.

Tree core sample results represent a limited sample number of nineteen trees from LS1, and although the diameter range and tree ages suggest that the hurricane force winds of the Olympic Blowdown of 1921 downed the trees in the area, more work needs to be done along the rest of the coast to confirm this conclusion. LS1 appears to contain the least disturbed ground surface along the Rialto coast, as evidenced by tree size, succession of vegetative understory and LiDAR imagery and tree size, but more work on the Sitka spruce age and size range may give a better understanding of the impact of this legendary storm and how it affected the coastline.

The marine terrace feature at Rialto is experiencing rapid changes due to wave action and erosive processes that hinder the ability to revisit radiocarbon collection sites over time and accurately measure terrace elevations. Between July 2018 and May 2019, radiocarbon sample sites 1 and 2 have been obscured by modern beach deposits that fully cover the terrace area. Radiocarbon sample site 3 has become more exposed over time as waves have eaten away at the terrace, causing sloughing of material and felling of benchmark trees used to create the terrace survey. This shows the dynamic properties of the beach environment and the power of tidal and storm waves at Rialto beach to alter the terrace over a relatively short period of time. The longevity of the marine terrace feature is unknown, thus conducting this study before the waves wash away evidence of possible marine uplift is important to understanding the regional response to subduction zone earthquakes. Re-occupying the marine terrace survey location and completing follow-up surveys to assess changes over time may show different depositional unit thicknesses as well as lend insight into the relationship between the old beach terrace and the hillslopes behind the terrace.

7. Conclusion

In studying Rialto Beach, complex geological processes that have shaped the study area have been documented through various methods. Using radiocarbon dating of wood found within the low elevation marine terrace from both old beach deposits and landslide material, landsliding has been dated at LS3 to less than 146-304 yrs calBP, the higher constraint for potential coseismic uplift. Further dendrochronology studies on trees killed during the landslide may be the key to determining the age of uplift and landsliding. The uplifted marine terrace contains old

beach material dated 500-600 yrs calBP overlain by landslide debris. The marine terrace may have been uplifted coseismically during the 1700 AD earthquake. It is capped by landslide deposits younger than 146-306 yrs calBP.

The geologic units within LS1 show presence of Vashon glacial and Olympia fm. interglacial units, with less permeable peat layers that may act as an aquitard and cause saturated upper units to slide. It is expected that these units are laterally continuous in the study area, and that the aquitard unit is present in LS3 above the marine terrace. It is reasonable that a large magnitude earthquake during high precipitation in winter could trigger sliding from the upper slopes.

Radiocarbon sample site 1 is a sample of Western red cedar dated to 800 yrs calBP in age. This shows that different plant species grew in the past environment, and suggests a landslide of around that date. Studying the Sitka spruce of LS1 to determine the age of the modern ground surface shows standing trees no older than 100 years in age, the time of the Great Olympic Blowdown of 1921. This legendary storm could likely have felled much of the pre-existing forest, making the nurse logs that cover much of the ground surface today. While investigating LS1 in the field, noted areas of standing water and saturated soils indicate high pore pressure and low strength, which could lead to slope failure on a slope denuded by winter storms. Intense mid-latitude storms therefore have the propensity to act as another cause of slope failure in the area.

Living trees cannot be used at this site for landslide dating because of recent blowdown and poor age/diameter correlation.

Landward erosion of the low-elevation terrace and tree-death along the coast indicate encroachment of the ocean towards the beach area and forested slopes. In the past 60 years, approximately 50 feet of coastal forest has been lost to rising seas and storm overwash (Jill Silver, pers. comm.). Projected sea-level rise and the storm-wave environment indicates that the area will continue to experience erosion of the terrace and death of the coastal forest.

8. Future Work

Further research at Rialto Beach will include more radiocarbon dating of organics within the marine terrace, including both landslide and old beach deposits as well as the grey clay layer with charcoal fragments, to constrain the age of potential uplift and timing of landslides. The low marine terrace may have been abruptly uplifted between 146-304 yrs calBP. The Marine Resources Committee has recently approved a proposal to collect and send more radiocarbon samples from the terrace to further investigate the date and origin of the feature.

Other researchers are currently studying uplift in the area, and a review of evidence found at nearby locations may lead to correlations or new methods of studying the low marine terrace at Rialto beach.

The marine terrace needs to be mapped further along the shoreline and changes to the 100-m portion of the terrace surveyed in this project may be re-surveyed to show erosional beach processes over time. Movement of beach material and shoreline encroachment is an important aspect of this study area.

Digging or coring behind the existing berm, within the wetland area, may give an idea of the landslide and beach unit thicknesses and may expose new unit contacts and dateable wood fragments. More landslide mapping and field-checking of landslides, especially those associated with radiocarbon data, will provide a clearer picture of the stratigraphy of the region. The thicknesses of the glacial and interglacial deposits found on LS1 may vary on other hillslopes and contain more constraining radiocarbon ages for dating the glacial till on top of the slopes.

Slope stability analysis of LS3, including dynamic loading assessment and factor of safety calculations, will add to visual and field observations of the area and contribute to the understanding of slope failure processes.

Careful elevation mapping of the top of old beach deposits compared to modern beach elevations may yield useful results for interpreting uplift and subsidence patterns.

9. References

Arnold, R., 1906, Geological reconnaissance of the coast of the Olympic Peninsula, Washington: Bulletin of the Geological Society of America, v. 17, p. 451-468.

Atwater, B.F., 1987, Evidence for great Holocene earthquakes along the outer coast of Washington state. Science: New Series, v. 236, no. 4804, p. 942-944.

Atwater, B.F., 2005, The Orphan Tsunami of 1700: Seattle, University of Washington Press. pp. 93-105

Ault Jr., C.R., 2014, The ghost forests of Cascadia: how valuing geological inquiry puts practice into place. Journal of Geoscience Education: vol, 62, no. 2, p. 158-165.

Bronk Ramsey, C., 1995, Radiocarbon calibration and analysis of stratigraphy: The OxCal program. Radiocarbon: vol. 37, no. 2, p. 425-430.

Bronk Ramsey, C., 2009, Bayesian analysis of radiocarbon dates. Radiocarbon: vol. 51, no. 1, p. 337-360.

Bronk Ramsey, C., 2017, Methods for summarizing radiocarbon datasets. Radiocarbon: vol. 59, no. 2, p. 1809-1833.

Danner, W.R., 1955, Geology of Olympic National Park. Seattle: University of Washington Press. 67 p.

https://www.earthmagazine.org/article/unlocking-cascadia-subduction-zones-secrets-peering-recent-research-and-findings.

Frankel, A., 2016, Modeling strong-motion recordings of the 2010 M_w8.8 Maule, Chile, earthqyake with high stress-drop subevents and background slip: Bulletin of the Seismological Society of America, v. 107, no. 1, p. 372-386.

Goldfinger, C., Nelson, C.H., Moren, A.E., Johnson, J.E., Patton, J.R., Karabanov, E., Gutierrez-pastor, J., Eriksson, A.T., Gracia, E., Dunhill, G., Enkin, R.J., Dallimore, A., Vallier, T., 2012, Turbidite event history- methods and implications for Holocene paleoseismicity of the Cascadia subduction zone, USGS Professional Paper, v. 1661-F, 171 pp.

Heusser, C.J., 1974, Quaternary vegetation, climate and glaciation of the Hoh river valley, Washington: Geological Society of America Bulletin, v. 85, p. 1547-1560.

Ludwin, R.S., Dennis, R., Carver, D., McMillan, A.D., Losey, R., Clague, J., Jonietz-Trisler, C., Bowechop, J., Wray, J., James., K., 2005, Dating the 1700 Cascadia earthquake: great coastal earthquakes in native stories: Seismological Research Letters, v. 76, n. 2, p. 140-148.

Li, S., Wang, K., Wang, Y., Jiang, Y., Dosso, S.E., 2018, Geodetically inferred locking state of the Cascadia megathrust based on a viscoelastic earth model: Journal of Geophysical Research: Solid Earth, v. 123, p. 8056-8072.

Mass, C., Dotson, B., 2010, Major extratropical cyclones of the northwest United States: historical review, climatology and synoptic environment. Monthly Weather Review; Washington, vol. 138, no. 7, pp. 2499-2501, 2503-2513, 2515-2518, 2522-2527.

McKay, P.J. and Terich, T.A., 1992. Gravel barrier morphology: Olympic National Park: Washington state, U.S.A.: Journal of Coastal Research, v. 8, no. 4, p. 813-829.

Miller, I.M., Morgan, H., Mauger, G., Newton, T., Weldon, R., Schmidt, D., Welch, M., Grossman, E. 2018, Projected Sea Level Rise for Washington State – A 2018 Assessment. A collaboration of Washington Sea Grant, University of Washington Climate Impacts Group, University of Oregon, University of Washington, and US Geological Survey. Prepared for the Washington Coastal Resilience Project. updated 07/2019

Ramos, M.D., Huang, Y., 2019, How the transition region along the Cascadia megathrust influences coseismic behavior: insights from 2-D dynamic rupture simulations: Geophysical Research Letters, v. 46, p. 1973-1983.

Rau, W.R., 1973, Geology of the Washington Coast between Point Grenville and the Hoh River: Washington Department of Natural Resources Geology and Earth Resources Division Bulletin No. 66.

Read, W., 2007, The Olympic Blowdown of January 29, 1921., https://climate.washington.edu/stormking/January1921.html

Satake, K., Shimazaki, K., Tsuji, Y., Udeda, K. (1996). Time and size of a giant earthquake in Cascadia inferred from Japanese tsunami records of January 1700: Nature, v. 379, p. 276-278.

Schulz, M., Lawrence, C., Muhs, D., Prentice, C., Flanagan, S., 2018. Landscape from the waves-marine terraces of California: United States Geological Survey Fact Sheet v. 2018-3002.

Spicer, R.C., 1986, Glaciers in the Olympic Mountains, Washington [M.S. Thesis]: Seattle, University of Washington, 157 p.

Tabor, R.W. and Cady, W.C., 1978. The structure of the Olympic Mountains, Washington- analysis of a subduction zone: Geological Survey professional paper 1033.

Thackray, G.D., 1996, Glacial and neotectonics deformation on the western Olympic peninsula, Washington [Ph.D. thesis]: Seattle, University of Washington, 167 p.

U.S. ARMY CORPS OF ENGINEERS, 1974. Draft EIS, Quillayute Harbor Project, 41 p.

Washington Department of Natural Resources LiDAR Portal WA Coast Topobathy 2014.

Wirth, E.A., Frankel, A.D., Vidale., D.E, 2017, Evaluating a kinematic method for generating broadband ground motions for great subduction zone earthquakes: application to the 2003 M_w8.3 Tokachi-Oki earthquake: Bulletin of the Seismological Society of America, v. 107, no. 4, p. 1737-1753.

Wirth, E.A. and Frankel, A.D., 2019, Impact of down-dip rupture limit and high-stress drop subevents on coseismic land-level changes during Cascadia megathrust earthquakes: Bulletin of the Seismological Society of America, V. 109, no. 6, p. 2187-2197.

10. Tables

Submitter Identification	Type	Process	Accession #	F Modern	Fm Err	δ13C Corr	Age	Age Err	δ13C	δ13C Source	Δ14C	CalBP(sigma1)	Elevation	Geologic Unit
KT 200-18 S-1	Plant/Wood	(OC) Organic Carbon	OS-147980	0.9208	0.0018	*	660	15	-23.89	Measured	-86.7	668-641 590-563	n/a	Qb
MAB 25-18 S-1	Plant/Wood	(OC) Organic Carbon	OS-147981	0.9354	0.0018	*	535	15	-27.98	Measured	-72.25	621-611 554-520	2.318	Qb
KT 32-18 S2	Plant/Wood	(OC) Organic Carbon	OS-148035	0.9761	0.0020	*	195	15	-25.4	Measured	-31.88	290-267 213-195 189-146 14	2.658	Qls
MAB 25-18 S5	Sediment Org	(OC) Organic Carbon	OS-148120	0.60200	0.00230	*	4080	30	-27.69	Measured	-402.9	4806-4760 4697-4673 4648-4514 4481-4445	n/a	Qb
MAB 25-18 S2	Charcoal	(OC) Organic Carbon	OS-148121	0.94110	0.00230	*	490	20	-24.18	Measured	-66.6	539-506	2.518	Qb
MAB 24-18	Plant/Wood	(OC) Organic Carbon	OS-148122	0.90040	0.00290	*	845	25	-27.36	Measured	-106.9	793-694	2.267	Qls
KT-32-18 S-1	Plant/Wood	(OC) Organic Carbon	OS-148123	0.97250	0.00210	*	225	15	-26.71	Measured	-35.44	304-281 170-151 5	2.108	Qls
KT-38-19 S-1	Plant/Wood	(OC) Organic Carbon	OS-149423	0.0437	0.0044	*	25,100	810	-27.73	Measured	-956.6	30890-27825	77.65	Qol

Table 1. Radiocarbon sample data collected from four sample locations at Rialto Beach. Ages have been calibrated to years calBP using OxCal 4.1.

Wood Identification					
Sample Name	Scientific Name	Common Name	Date Analyzed	Location Description	Citation
CB 01-19-S1 Rialto	Thuja plicata	Western red cedar	6/13/2019	Recovered from radiocarbon sample site 1 , within low elevation marine terrace landslide deposit	Personal communication, Ed Espinoza, USFS Forensics Laboratory, Ashland, OR; personal communication, Michael Weissman, USFS Madison, Wisconsin
KT-39-19-S1B Rialto Beach La Push, WA	Picea sitchensis	Sitka spruce	6/13/2019	Found within northern gully of LS1 in interglacial layer, dated >48ka	Personal communication, Ed Espinoza, USFS Forensics Laboratory, Ashland, OR; personal communication, Michael Weissman, USFS Madison, Wisconsin

Table 2. Wood samples collected at Rialto Beach identified by USFS Forensics Laboratory ICPMS and through visual identification at USFS Wisconsin Laboratory.

Growth Variables	n	Linear Regression	R2 Value	Age Range (yrs)	Diameter Range (cm)	Average age	Average Diameter (cm)	Figure no.
All trees	19	y= 0.2043x+58.545	0.3018	58.5	131.06	81	105	31
Trees growing on ground with low sunlight availability	4	y= 0.154x+67.222	0.3512	25	103.12	87.5	131.7	32
Trees growing on ground with high sunlight availability	4	y= 0.5669x+27.864	0.7465	52.5	80.01	74	81.6	33
Trees growing on nurse log with low sunlight availability	5	y= 0.2961x+46.335	0.6262	35	125.22	84	111.73	34
Trees growing on nurse log with high sunight availability	6	y= -0.0744x+92.15	0.061	4.5	50.80	83.6	118.92	35
Trees growing on low bench	7	y= 0.0646x+69.088	0.0155	47.5	95.5	74	82.7	36
Trees growing on middle bench	7	y= 0.2296x+62.832	0.5051	21	100.33	84.5	112.59	37
Trees growing on top bench	5	y= 0.3462x+31.186	0.9981	39.5	108.20	74	92.4	38

Table 3. Calculated data from tree core diameter and averaged ages from 19 trees sampled on LS1 (Figure 30; Appendix 1-A).

11. Figures

Figure 1. Map showing location of Rialto Beach, on the northwest portion of the Olympic Peninsula, Washington State. Map made using the Washington State Department of Natural Resources Geologic Portal, January 2019.

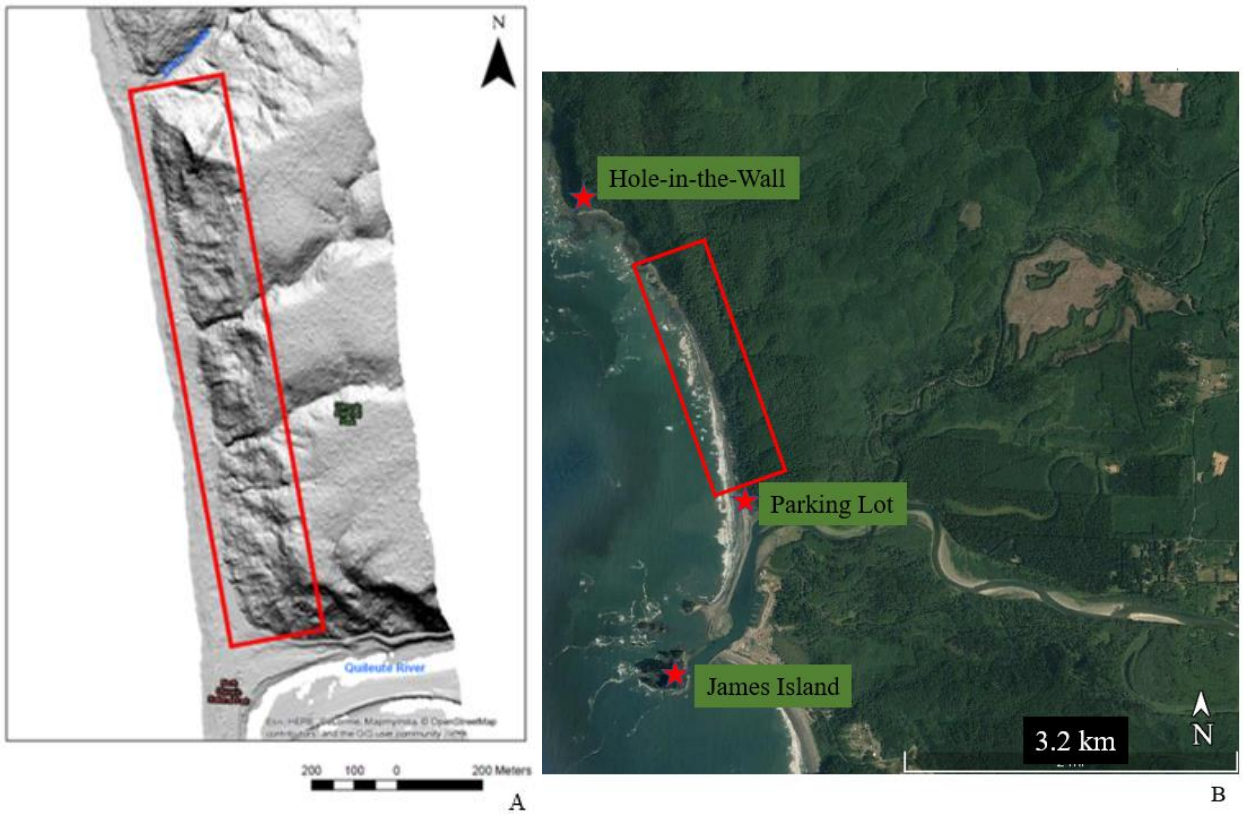

Figure 2(A). Site map, red box indicates the study area, including the forested hillslopes and the low elevation marine terrace. Adapted from LiDAR imagery, Washington state Department of Natural Resources LiDAR portal, 2014. (B) Map showing location of Rialto beach parking area, James Island and the Hole-in-the-Wall at the northern-most end of Rialto Beach. The red box indicates the study area. Image adapted from Google Earth.

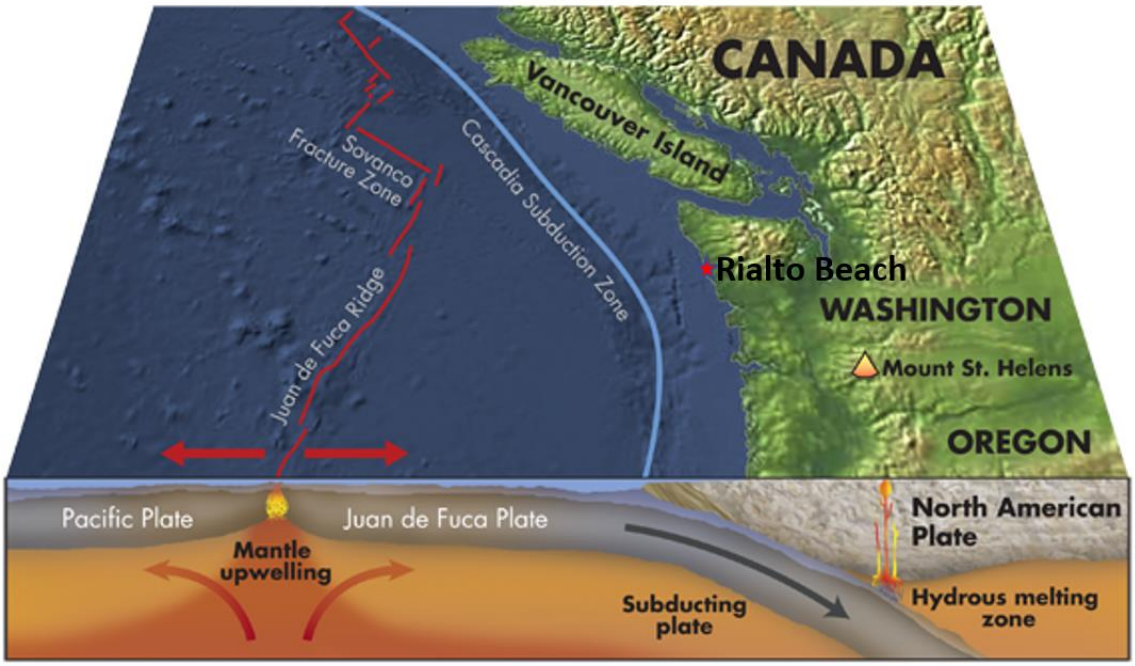

Figure 3. Image of the Cascadia Subduction Zone, showing the subducting Juan de Fuca Plate moving beneath the North America plate, creating the accretionary wedge responsible for the creation of the Olympic Mountains, bedrock of the Olympic Peninsula, and earthquake hazards along the Pacific coast. Image from Earth Magazine, 2019. www.earthmagazine.org.

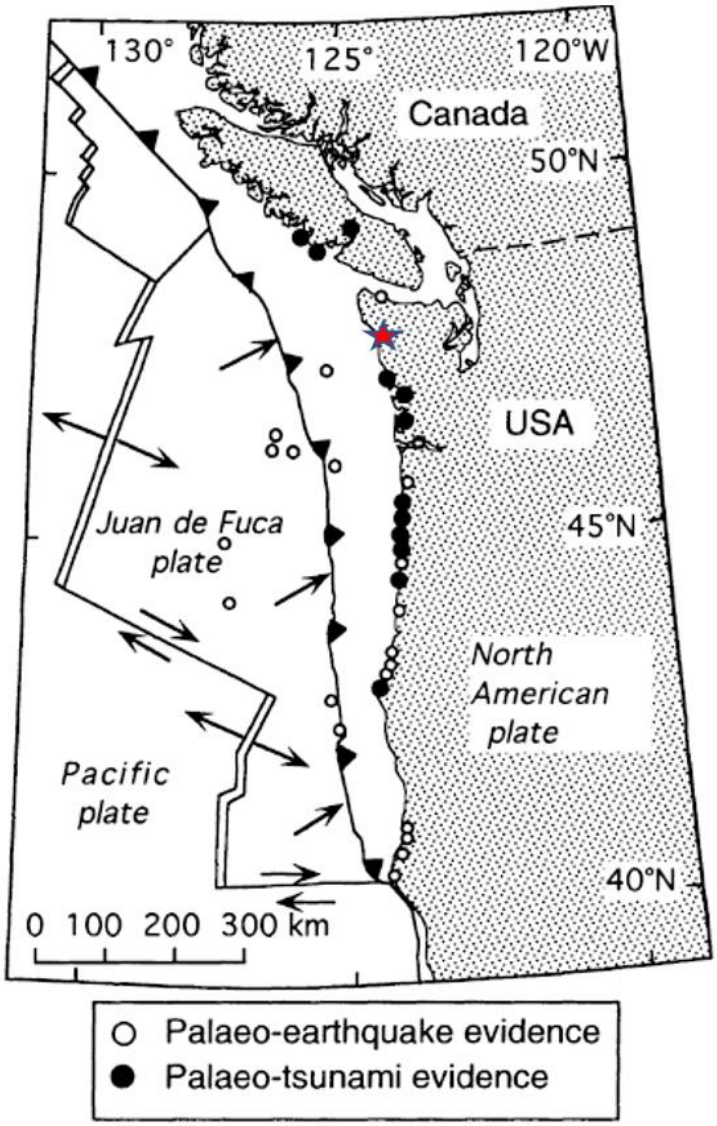

Figure 4. Map showing areas with evidence of the 1700 A.D. Cascadia subduction zone earthquake. The red star represents the approximate location of Rialto Beach. Note the lack of paleo earthquake and tsunami evidence in the study area. Image adapted from Satake et al., 1996.

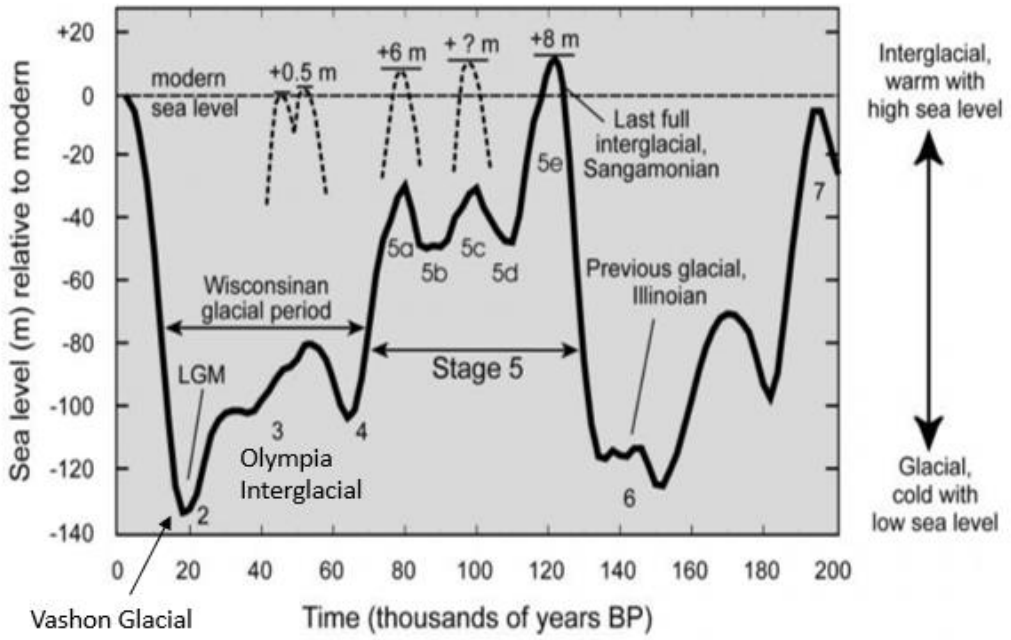

Figure 5. Oxygen Isotopic records showing global ice volumes and sea levels for the past 200,000 years. Rialto beach contains deposits from MIS-3 (Olympia interglacial) and MIS-2 (Vashon glacial). (Thackray, 1996). Figure adapted from Martinson et al., 1987 by *Figures for the Geology of the Virginia Coast*.

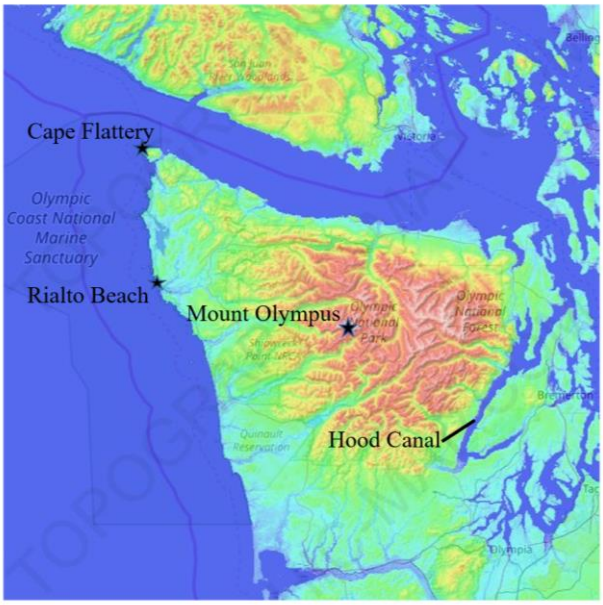

Figure 6. Elevation map showing locations of Mount Olympus, Hood Canal, and Cape Flattery, with the study area starred. Figure adapted from https://en-gb.topographic-map.com/maps/sihb/Olympic-National-Park/

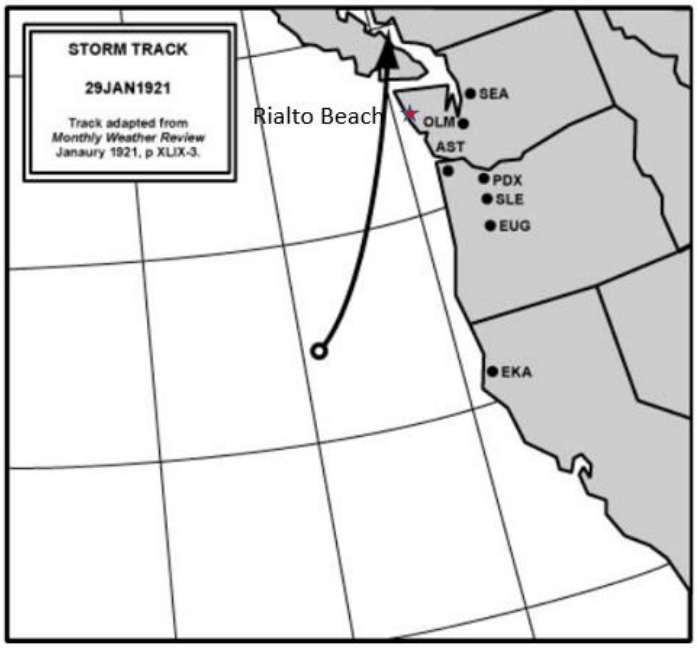

Figure 7. Storm track of the "Olympic Blowdown of 1921". The red star indicates the approximate location of the study area to illustrate proximity to storm path. Adapted from https://climate.washington.edu/stormking/January1921.html

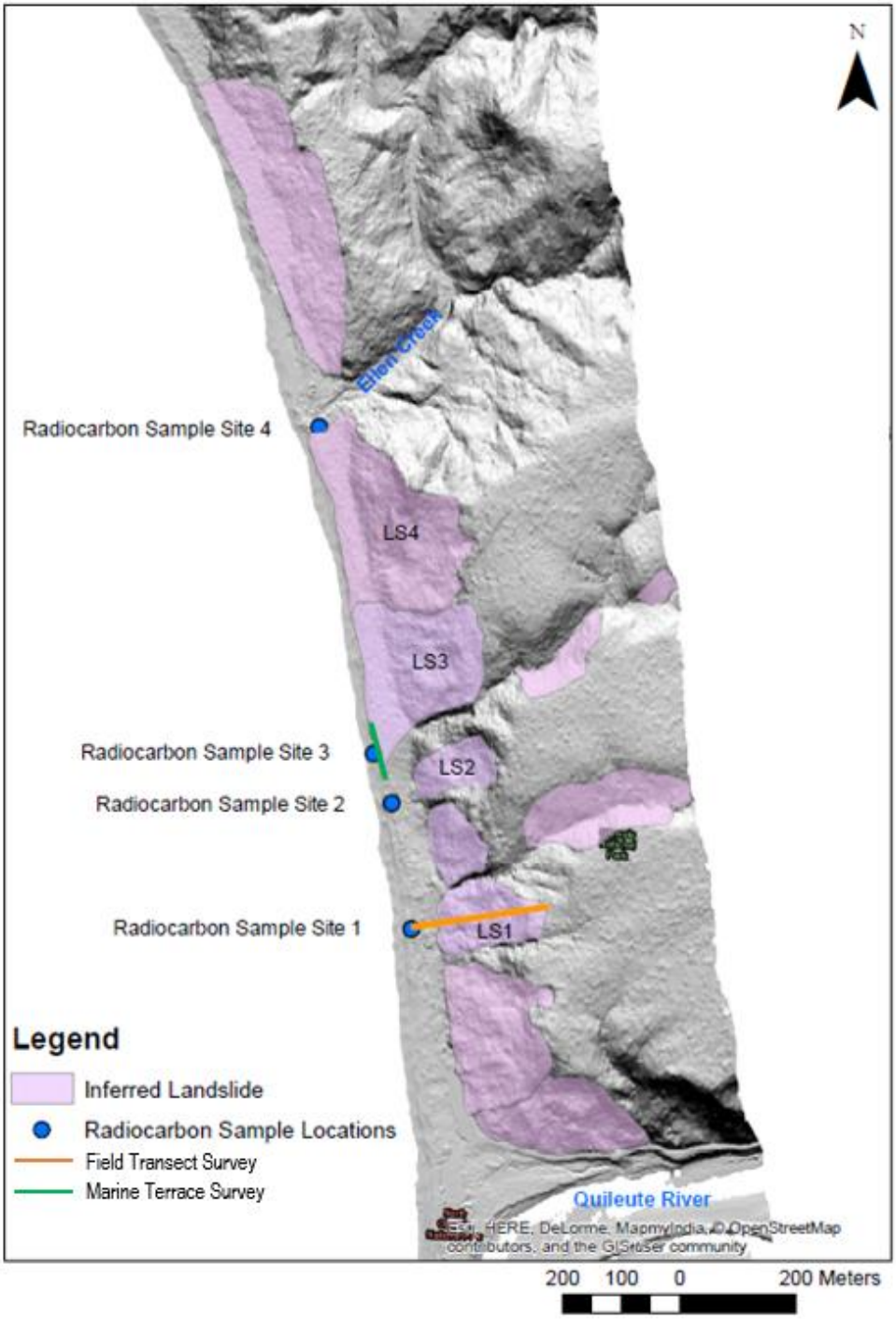

Figure 8. LiDAR map showing radiocarbon sample collection sites, the location of the field transect survey, the location of the marine terrace survey and inferred landslide locations. Labeled landslides have been studied in the field and/or are associated with radiocarbon ages, and those without labels have been identified by gemorphic features in LiDAR. Adapted from Washington State Department of Natural Resources Geologic Portal, 2014.

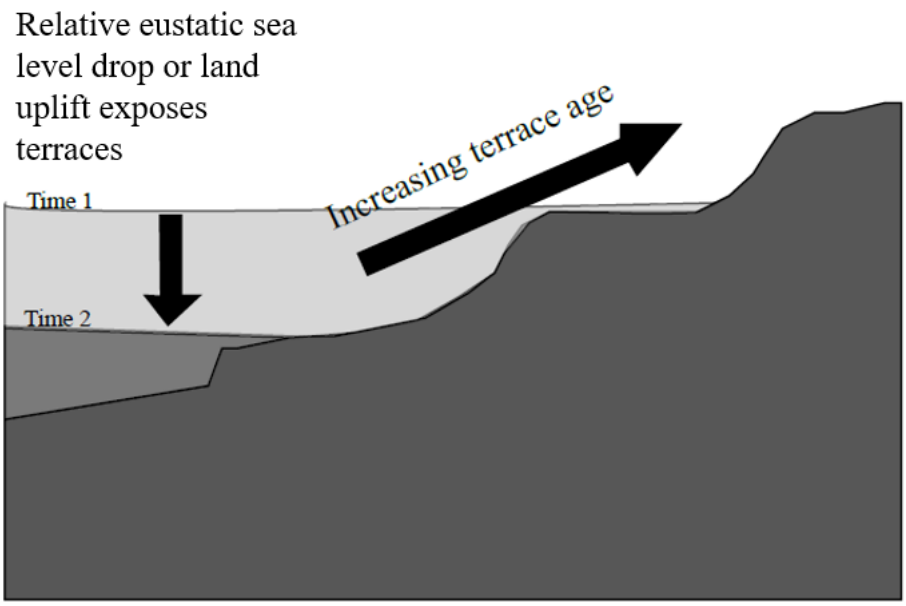

Figure 9. Schematic drawing showing the formation of a marine terrace.

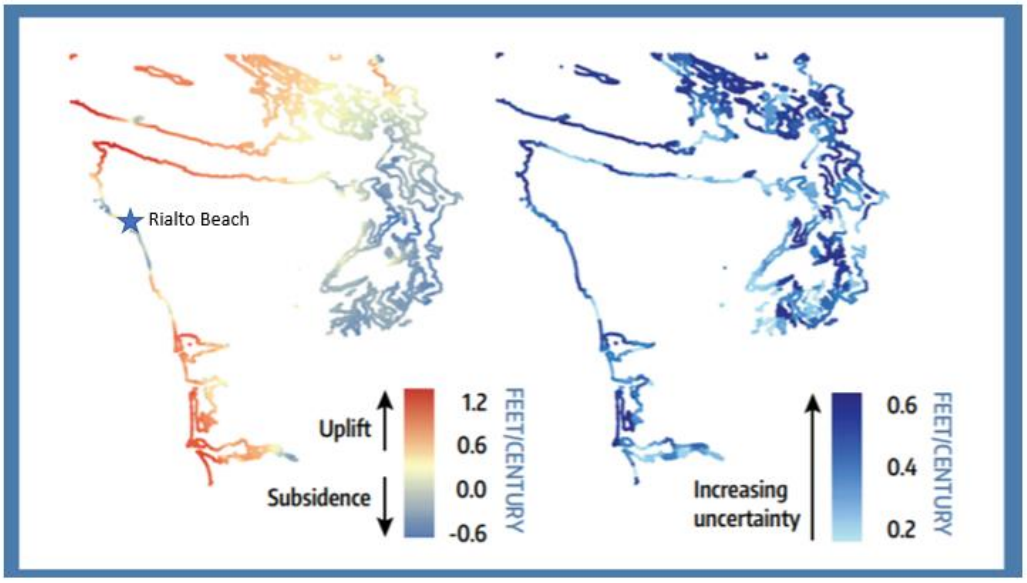

Figure 10. Uplift and subsidence measurements indicating that the study area is currently experiencing subsidence. Figure adapted from Miller et al., 2018.

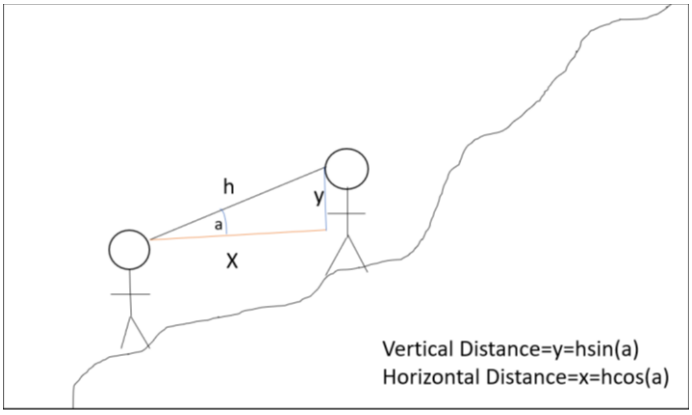

Figure 11. Diagram of field survey method including the basic trigonometry used to calculate changes in vertical and horizontal distance. This was used to construct the topographic profile of the cross section of the hillslope terminating at radiocarbon sample location 1.

A B

Figure 12(A) University of Washington student Elizabeth Davis collecting a tree core from a Sitka spruce at Rialto Beach. (B) Mounted, glued and labeled tree cores tied up with string to ensure no warping occurs during the drying process.

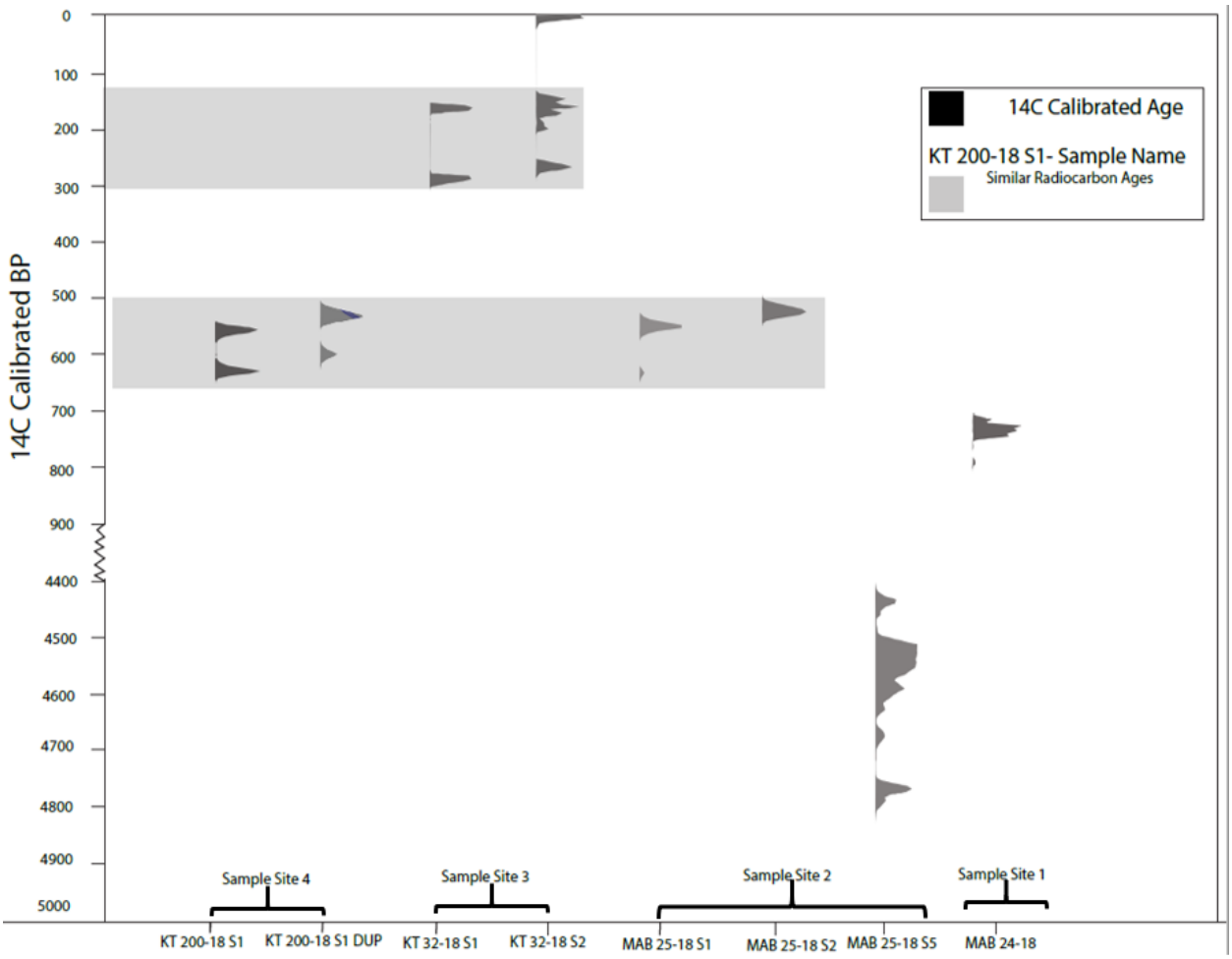

Figure 13. Graph showing radiocarbon sample data ranges in calibrated years BP. All samples were calibrated using Oxcal and ranges show one sigma (95.4%) probability. The grey bars represent radiocarbon samples with overlapping age ranges. Samples from sites 2 and 4 are from older beach deposits. Samples from sites 1 and 3 are from landslide deposits.

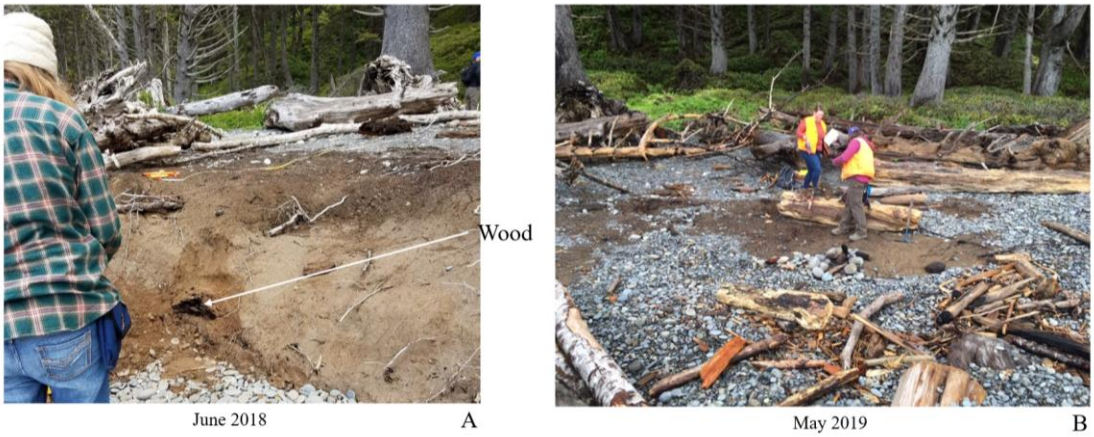

Figure 14(A). Wood collected from a landslide deposit at radiocarbon sample site 1. Large chunks of Western red cedar were entrained in the landslide deposit. Photo by K. Troost. (B) Less than a year later, the area is covered by modern beach deposit and driftwood.

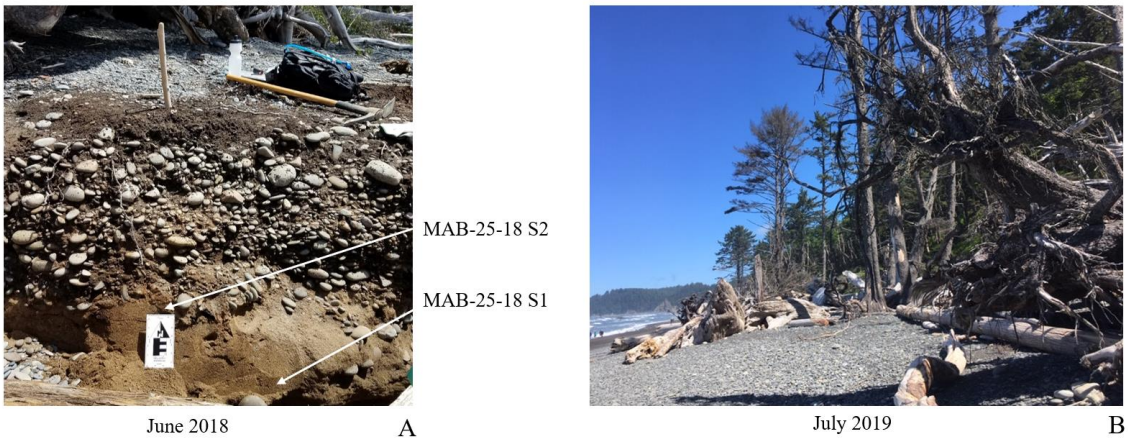

Figure 15(A) Radiocarbon sample site 2, old beach deposit sample location, showing clean sand with coarse pebble beach deposit above. Charcoal sample collected from top and bottom of deposit. Photo by K. Troost. (B) Sample location completely covered by modern beach over a year later.

Figure 16(A) Radiocarbon sample site 3 sampled in June of 2018, Austin Rains points to sampled wood fragments entrained within a landslide deposit. (B) Close up of wood sampled for radiocarbon dating. Photos by K. Troost.

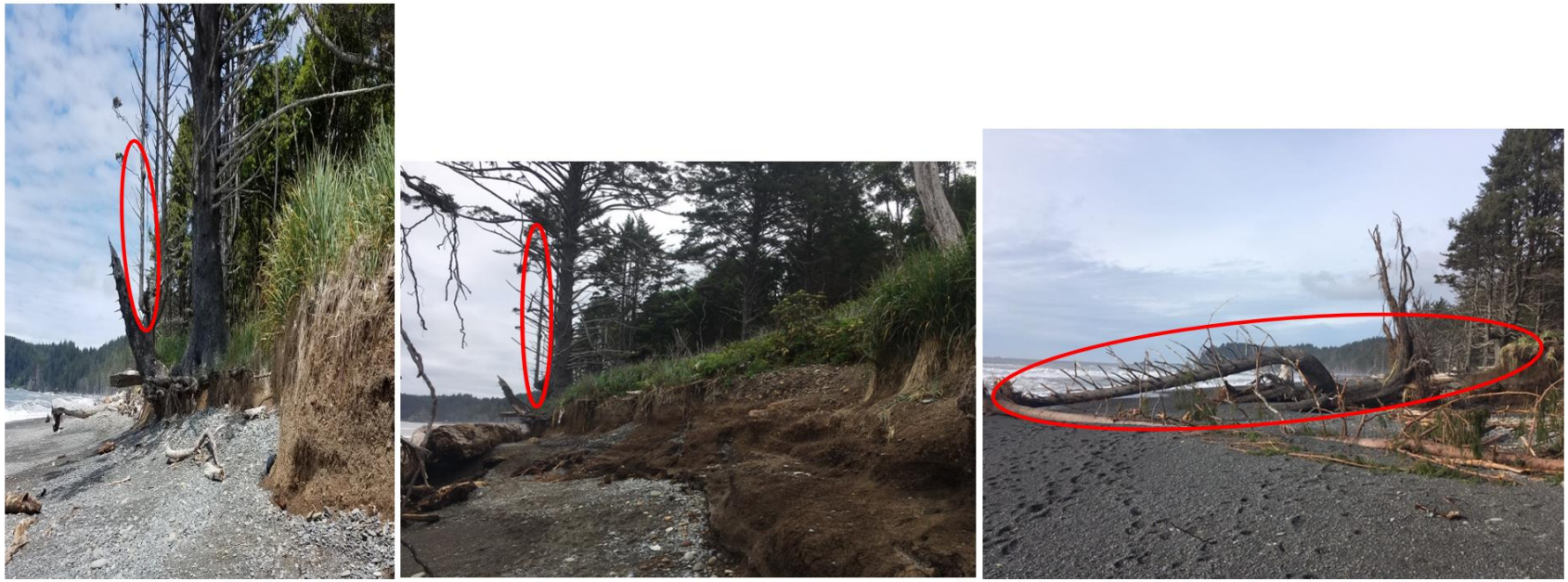

Figure 17 (A) Radiocarbon sample site 3 during sample selection, photo taken looking north along the beach. The Sitka spruce circled in red acted as a benchmark for the marine terrace survey. Photo by K. Troost. (B) Photo from the same view taken July 2019, showing more exposure of the marine terrace due to wave action. (C) In October of 2019 the benchmark tree had fallen onto the beach and the marine terrace was eroding quickly due to increased wave action.

Figure 18. Radiocarbon sample site 4. The sample was collected from old beach deposit near the mouth of Ellen creek on the left bank. Photo by K. Troost.

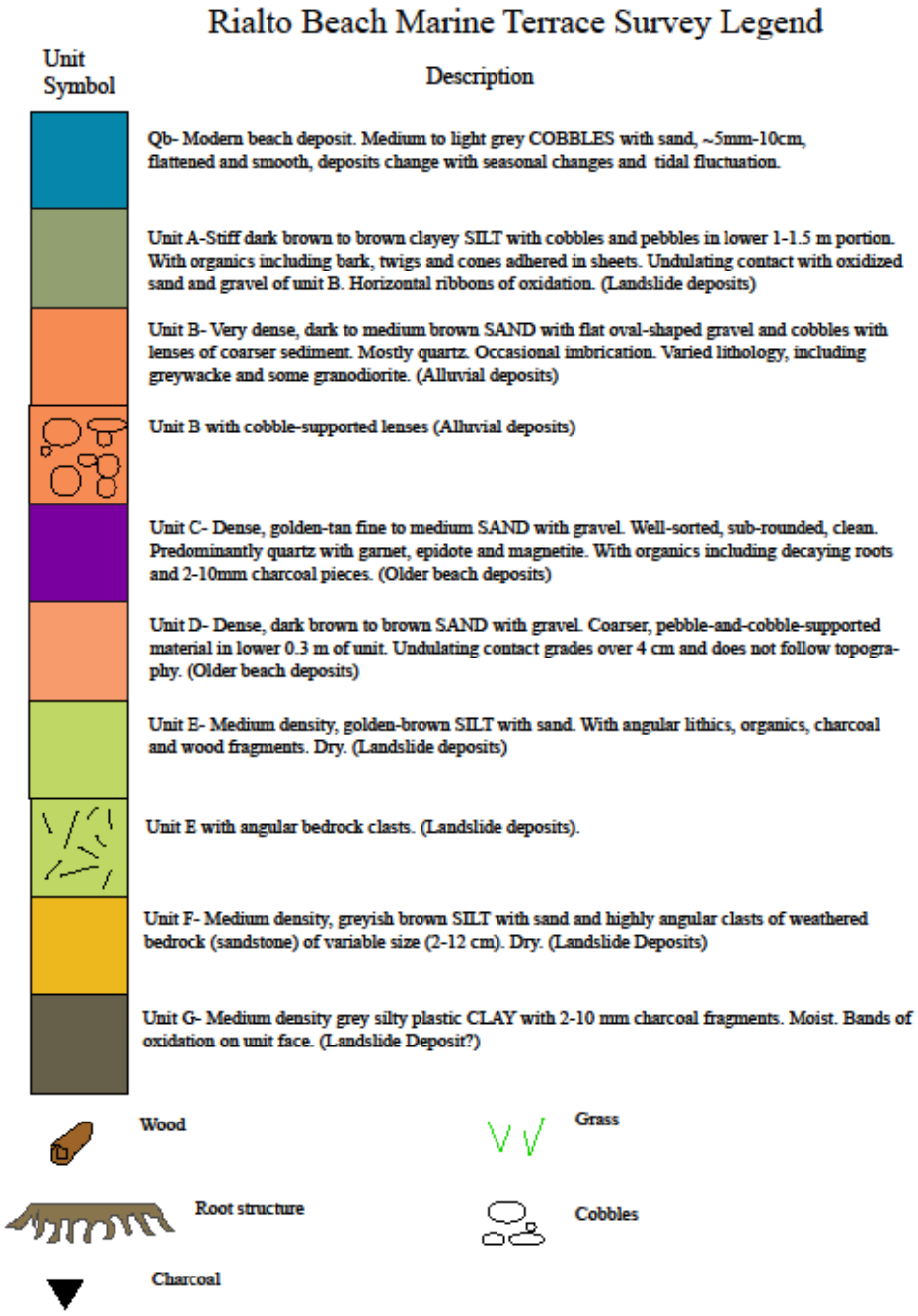

Figure 19. Legend showing symbology for the survey of the low-elevation marine terrace at Rialto beach, survey date July 7-8, 2019. See Figures 20-25.

Figure 20. Sketch of west face of low elevation marine terrace from south to north (see map Figure 11). Modern beach deposits are banked up against the terrace. 0 on drawing=MSL based on CORS Neah Bay, WA.

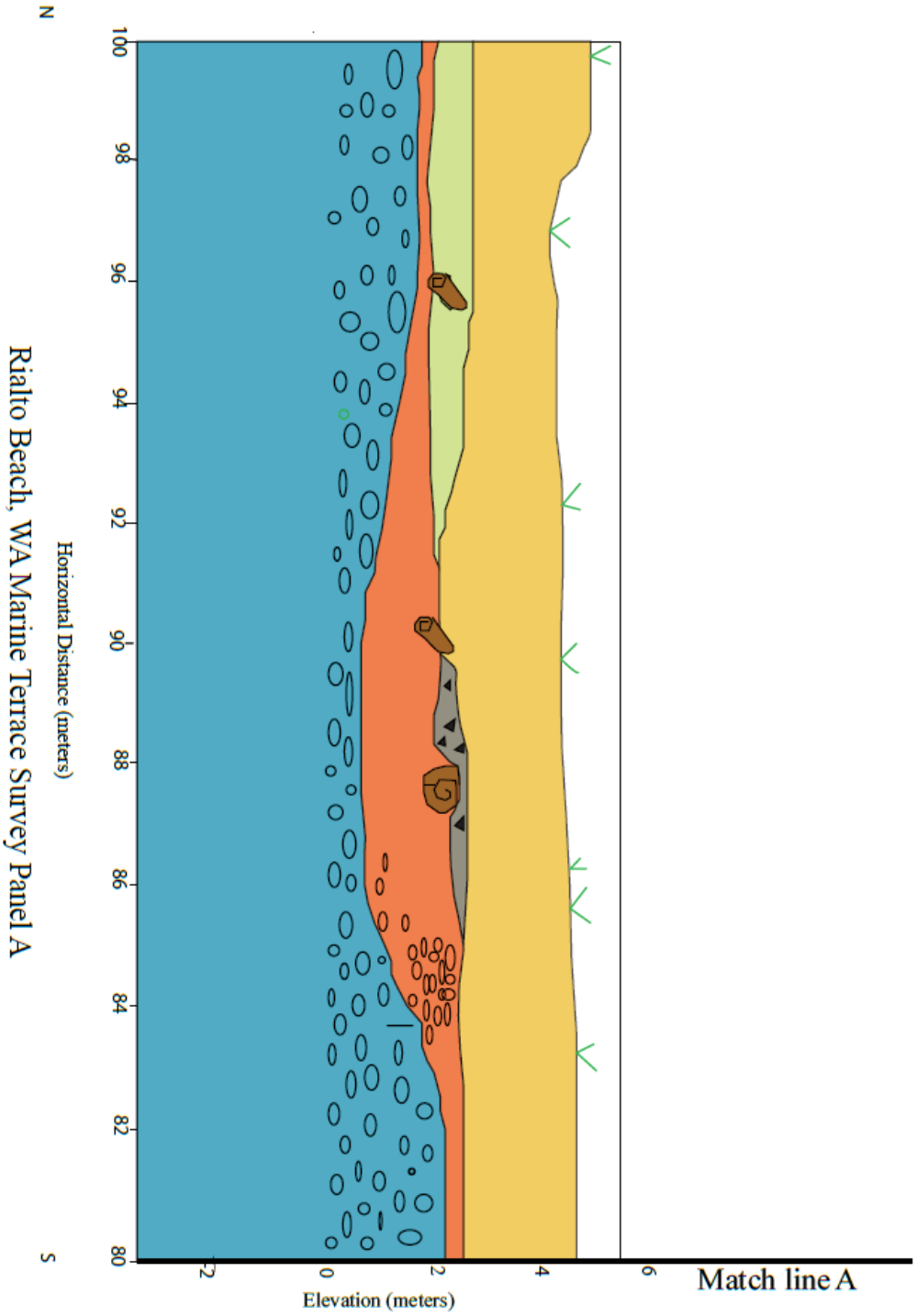

Figure 21. Marine terrace survey panel A. 0 on drawing=MSL based on CORS Neah Bay, WA. Modern beach deposits are banked up against the terrace edge. See legend Figure 18.

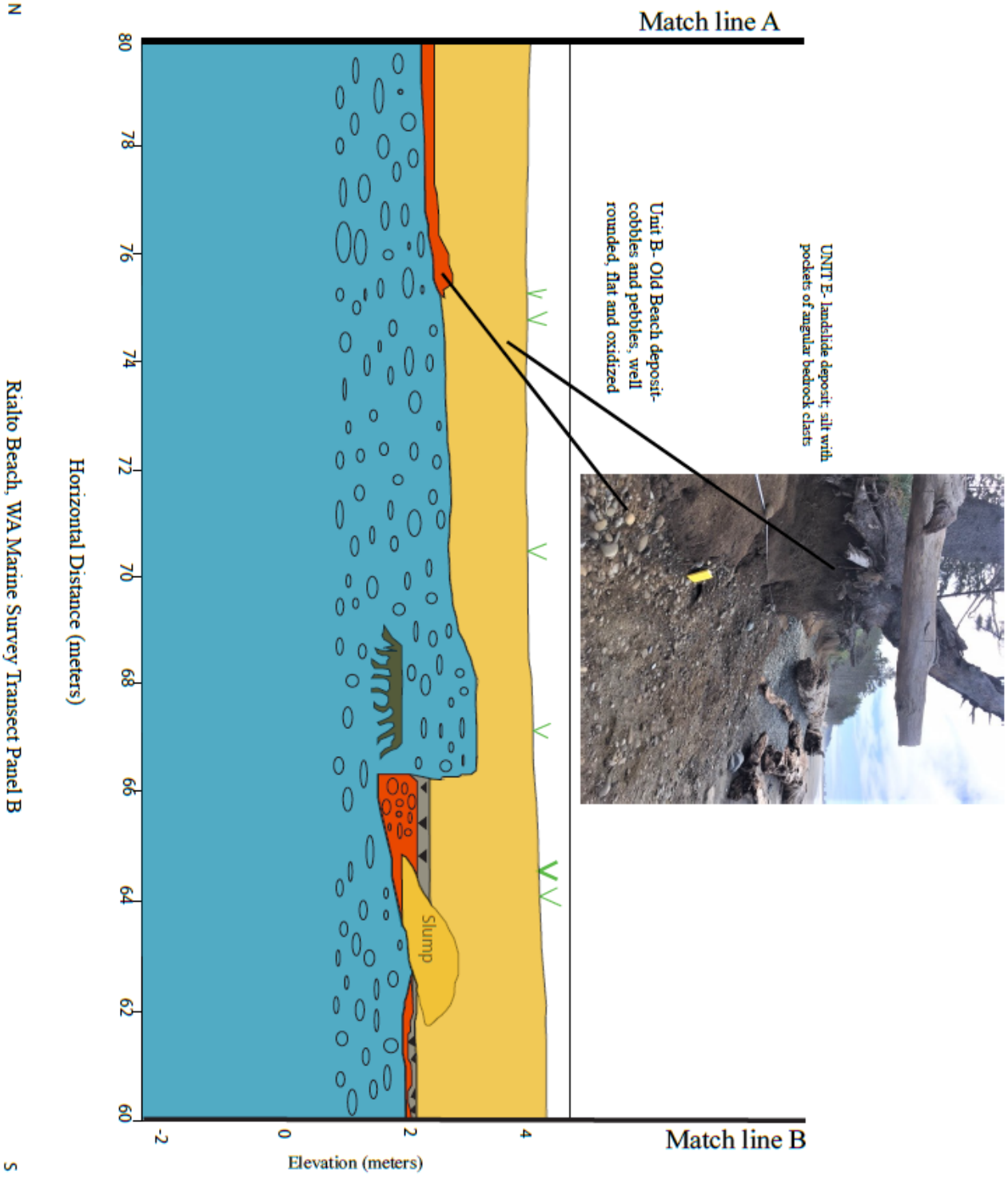

Figure 22. Marine terrace survey panel B. 0 on drawing=MSL based on CORS Neah Bay, WA. Modern beach deposits are banked up against the terrace edge. See legend Figure 18.

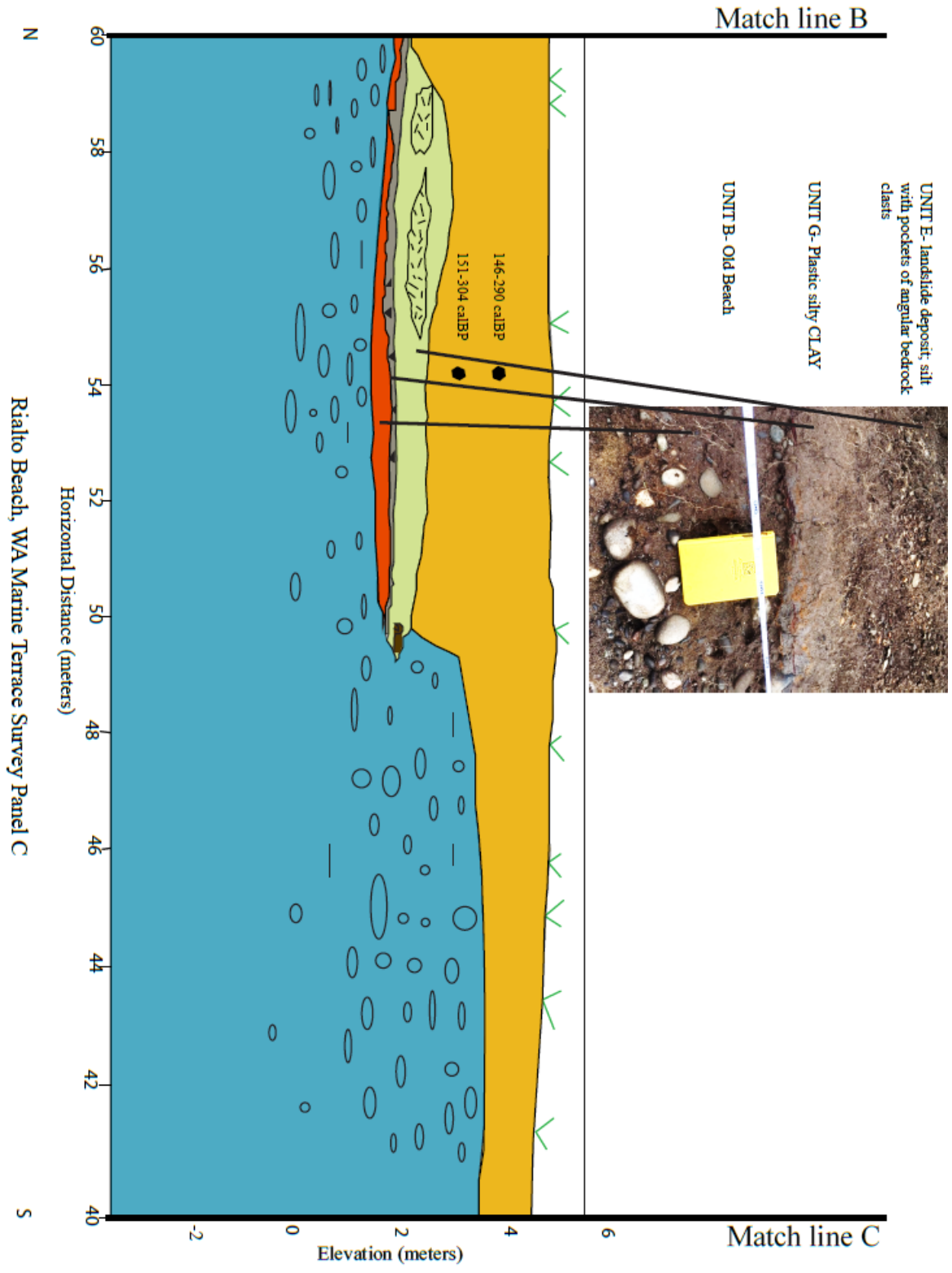

Figure 23. Marine terrace survey panel C. 0 on drawing=MSL based on CORS Neah Bay, WA.. Modern beach deposits are banked up against the terrace edge. See legend Figure 18.

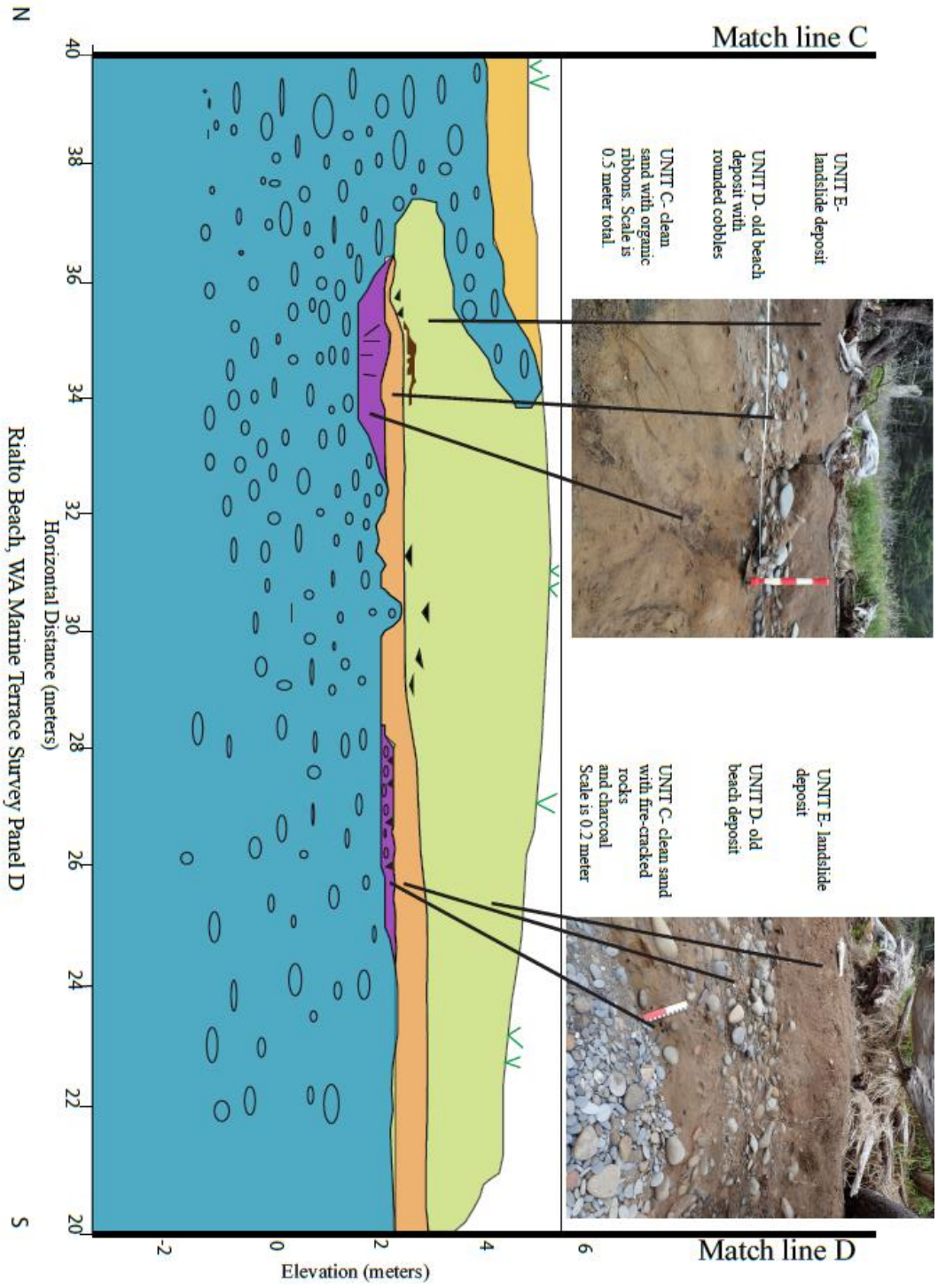

Figure 24. Marine terace survey panel D. 0 on drawing=MSL based on CORS Neah Bay, WA.. Modern beach deposits are banked up against the terrace edge. See legend Figure 18

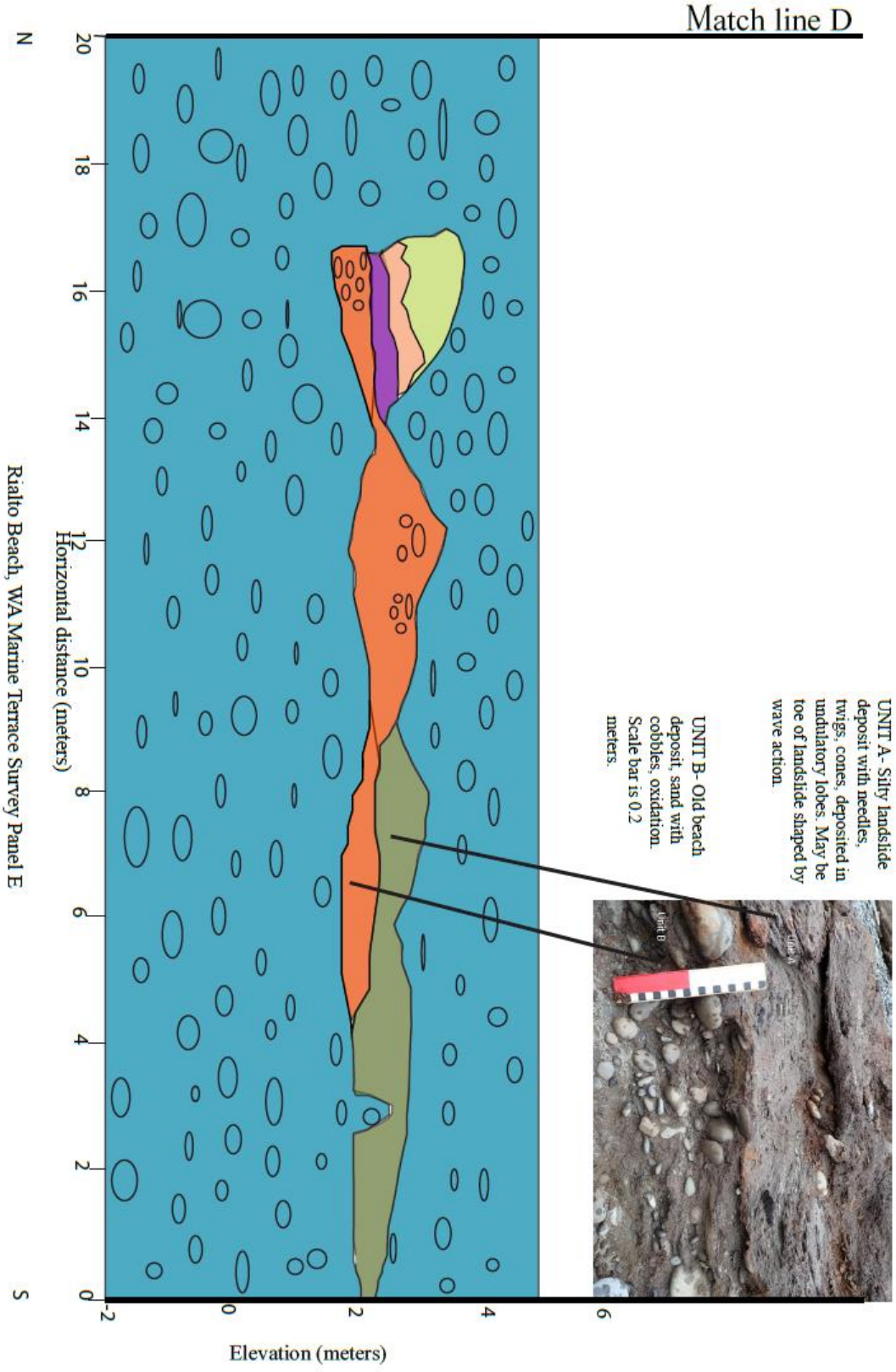

Figure 25. Marine terrace survey panel E. 0 on drawing=MSL based on CORS Neah Bay, WA.. Modern beach deposits are banked up against the terrace edge. See legend Figure 18.

Figure 26. Marine terrace exposure on October 23, 2019, showing landslide debris dated to ~300 years calBP overlying aquitard clay layer, which caused multiple seeps along the terrace face. Below this is Old beach, dated to be between 500-600 years calBP.

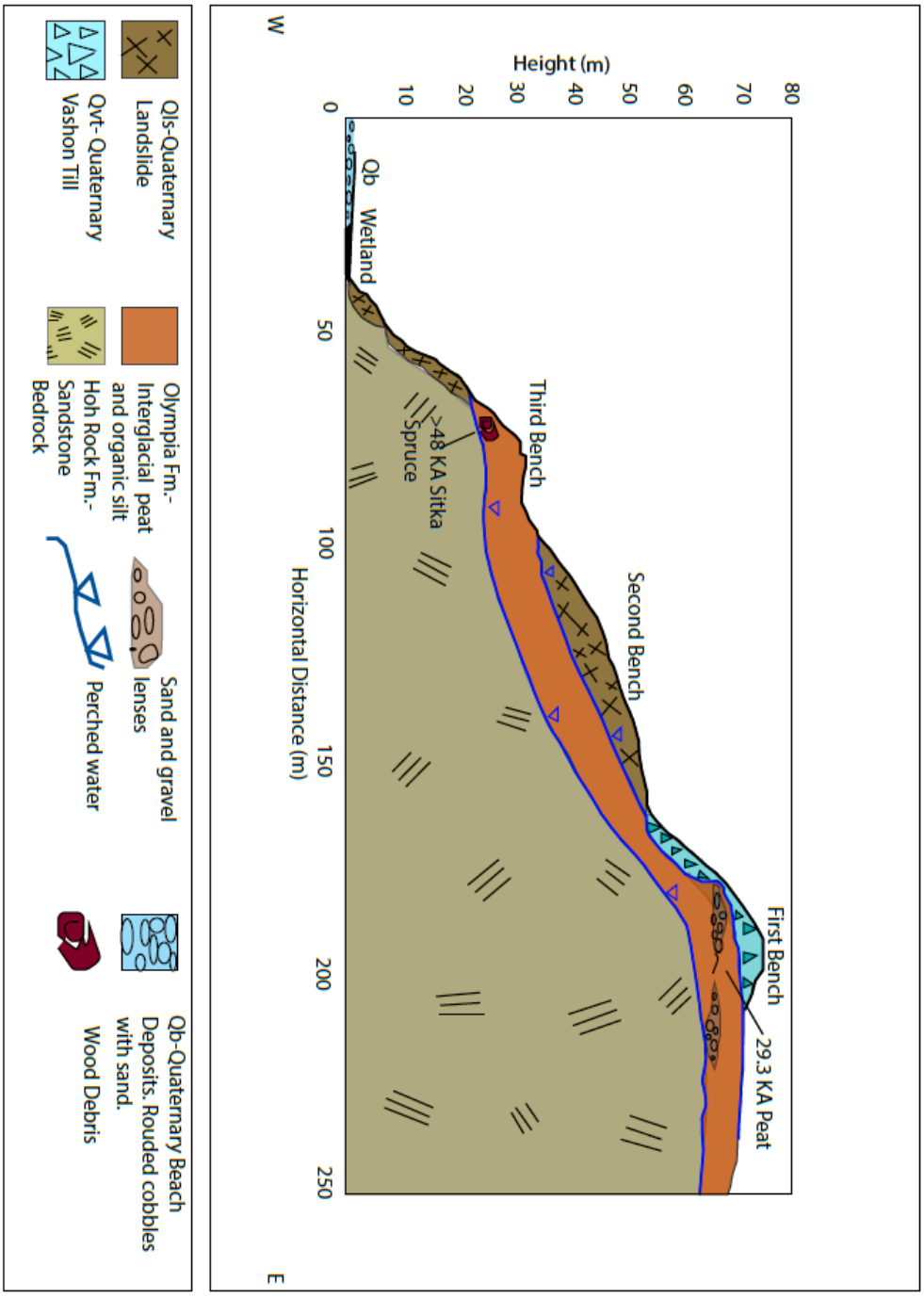

Figure 27. Sitka spruce root wad with glacial till entrained within the roots, at an elevation of 55 meters on LS1.

Figure 28. Sitka spruce root wad with glacial till entrained within the roots, at an elevation of 55 meters on LS1.

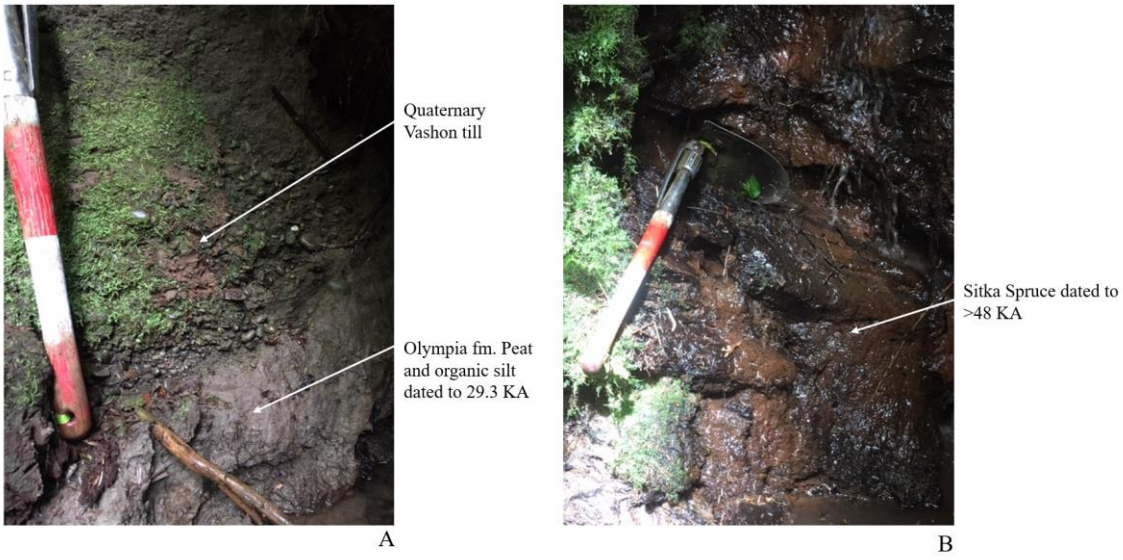

Figure 29. Two images from the interglacial unit buttressing the hillslope of LS1, within the northernmost ravine. 1 (A) Contact between glacial till and interglacial peat dated to 29.3 years ka, within an incised portion of the stream at an elevation of 67 meters. (B) Sitka spruce dated >48,000 years ka found in same gully at elevation of ~20 meters.

.

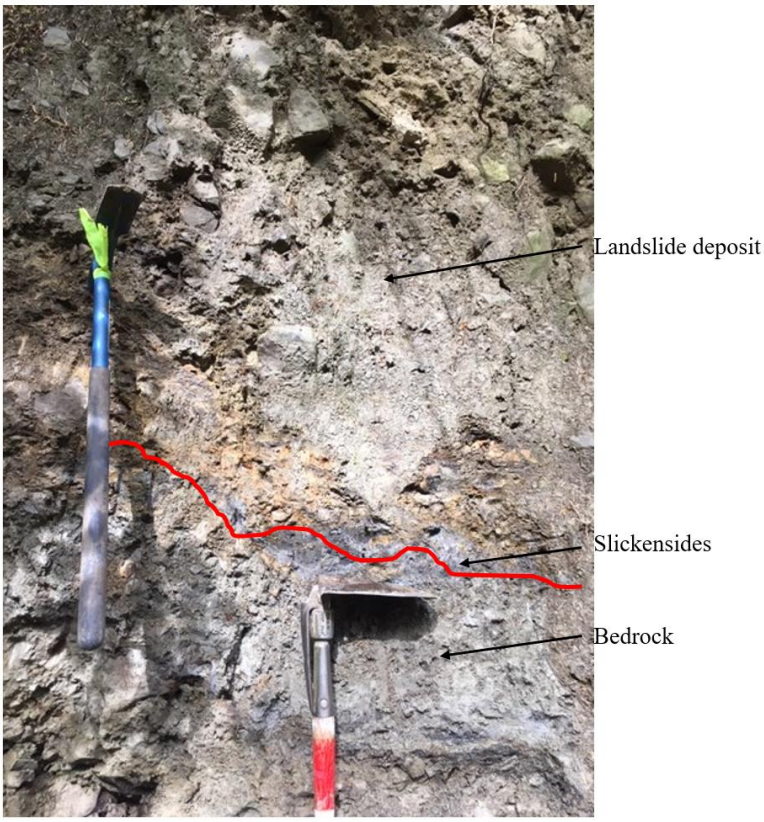

Figure 30. Photograph of contact between bedrock and inferred landslide deposit. Slickensides are present on the undulatory plane. This exposure is located in the northern ravine of LS1, at an elevation of 8 m.

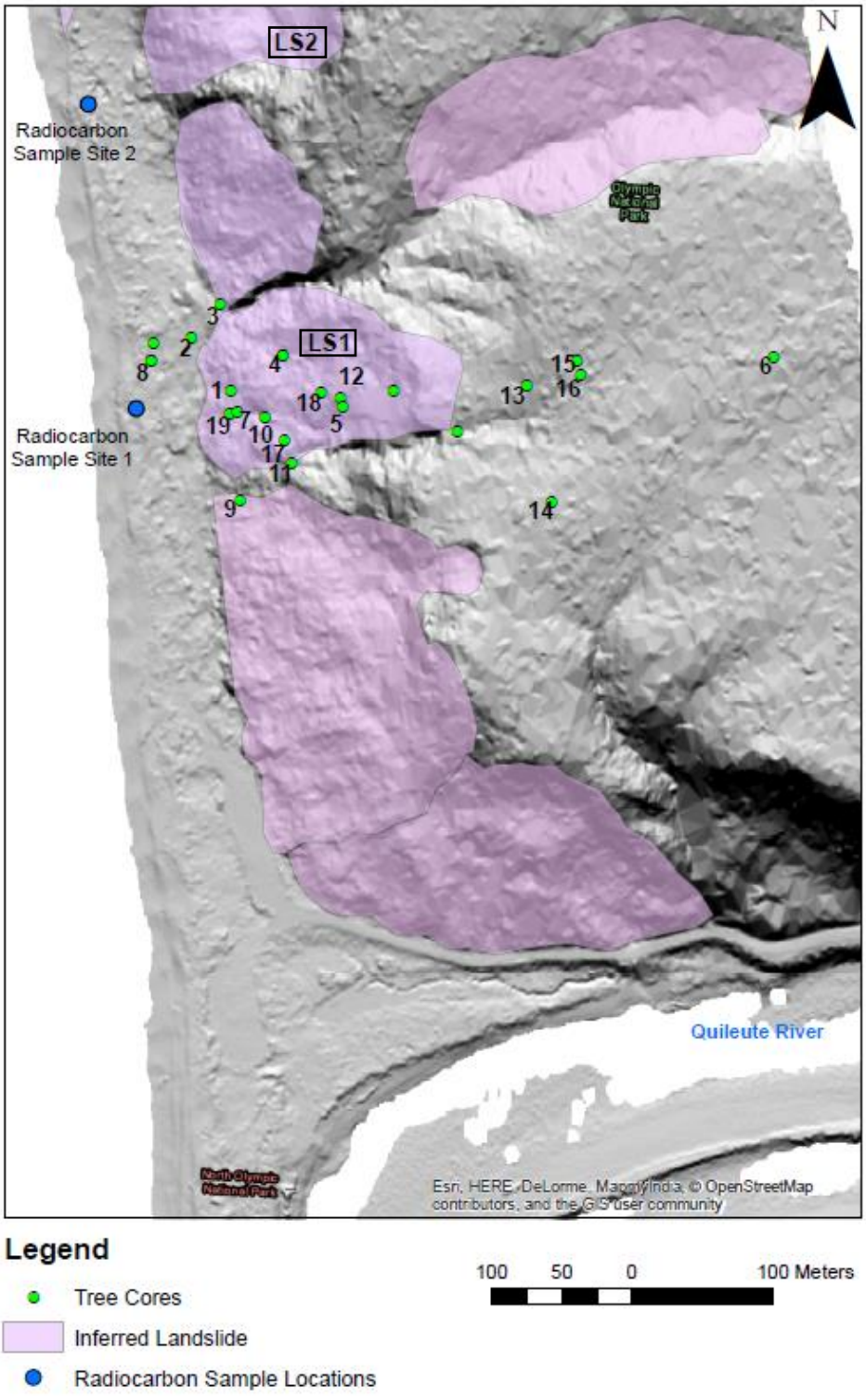

Figure 31. Rialto Beach LiDAR image showing tree core locations (see table 1-A for corresponding tree core descriptions).

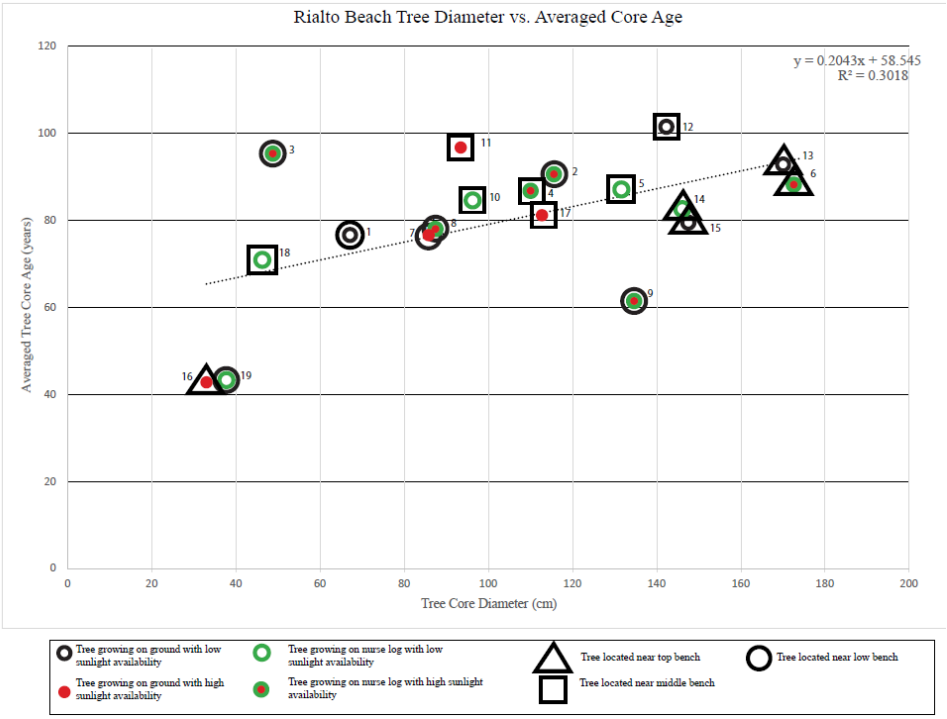

Figure 32. Tree diameter vs. tree age as counted from two averaged tree cores for each Sitka spruce tree. Nineteen trees were successfully cored on LS1 (see Figure 29). Other variables include amount of sunlight based on surrounding tree canopy, if the tree was growing from a nurse log, and closest bench feature. To average the tree age, two cores were taken from each tree approximately 90° from each other and the counted ages were averaged.

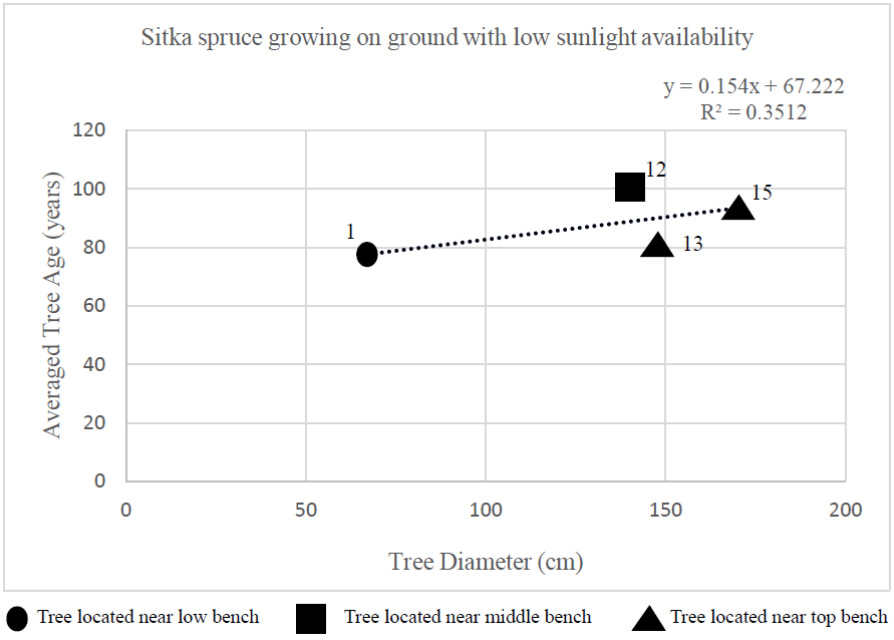

Figure 33. Graph of diameter vs. age of four trees growing on the ground with low sunlight availability on LS1 (see map Figure 29). Tree descriptions shown in table 1-A.

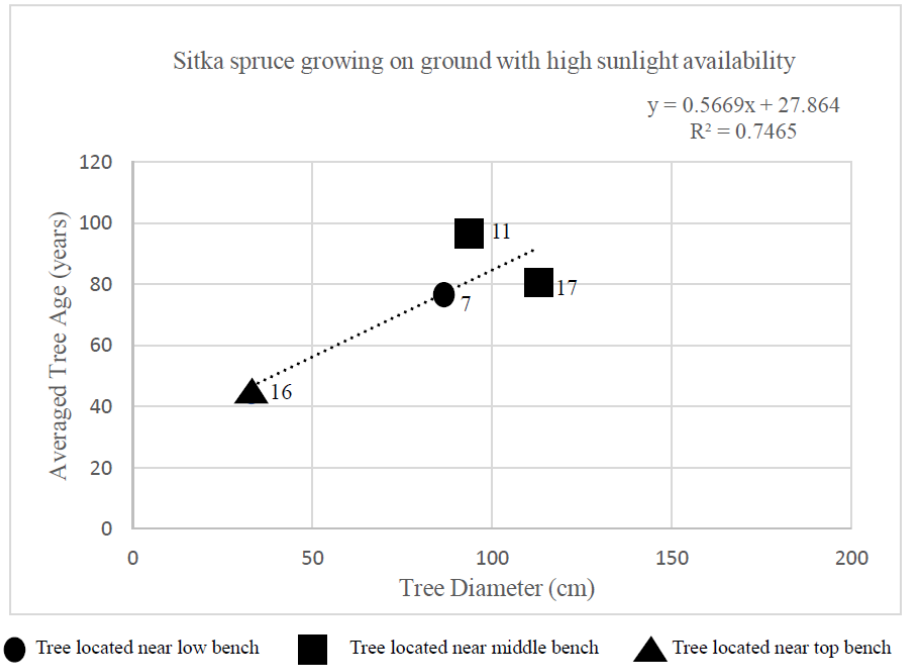

Figure 34. Graph of diameter vs. age of four trees growing on the ground with high sunlight availability on LS1 (see map Figure 29). Tree descriptions shown in table 1-A.

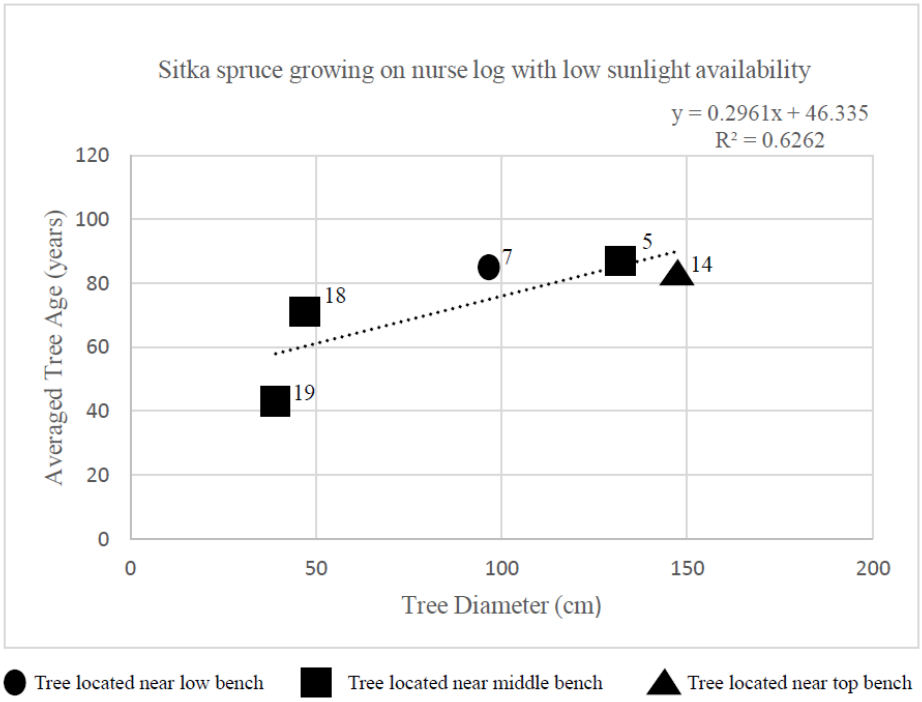

Figure 35. Graph of diameter vs. age for five trees growing on nurse logs with low sunlight availability on LS1 (see map Figure 29). Numbers correlate with tree descriptions in table 1-A.

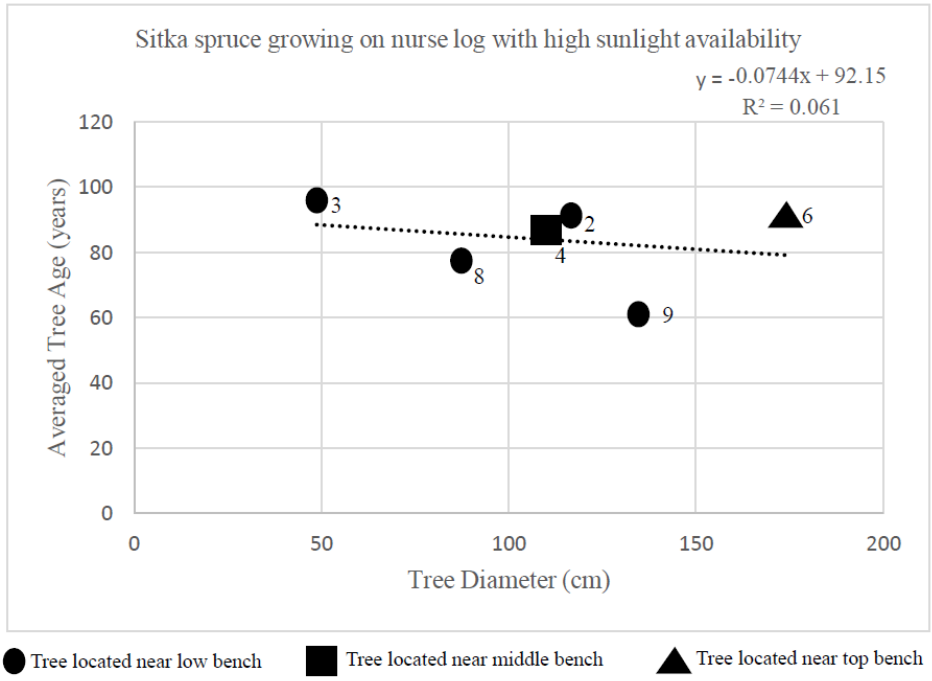

Figure 36. Graph of diameter vs. age for six trees growing on nurse logs with high sunlight availability on LS1 (see map Figure 29). Numers correlate with descriptions in table 1-A.

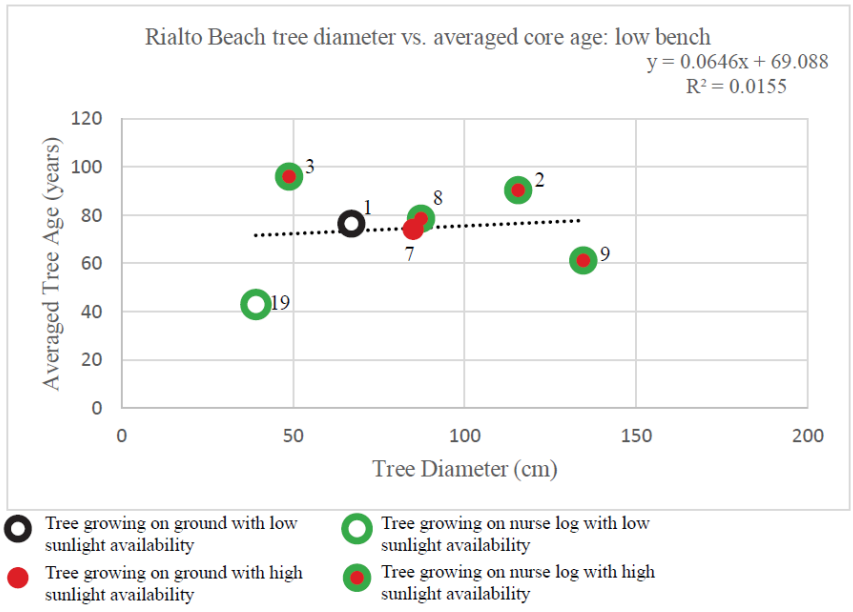

Figure 37. Graph of tree diameter vs. averaged tree age of seven trees growing on or near the low bench of LS1 (see map Figure 29).

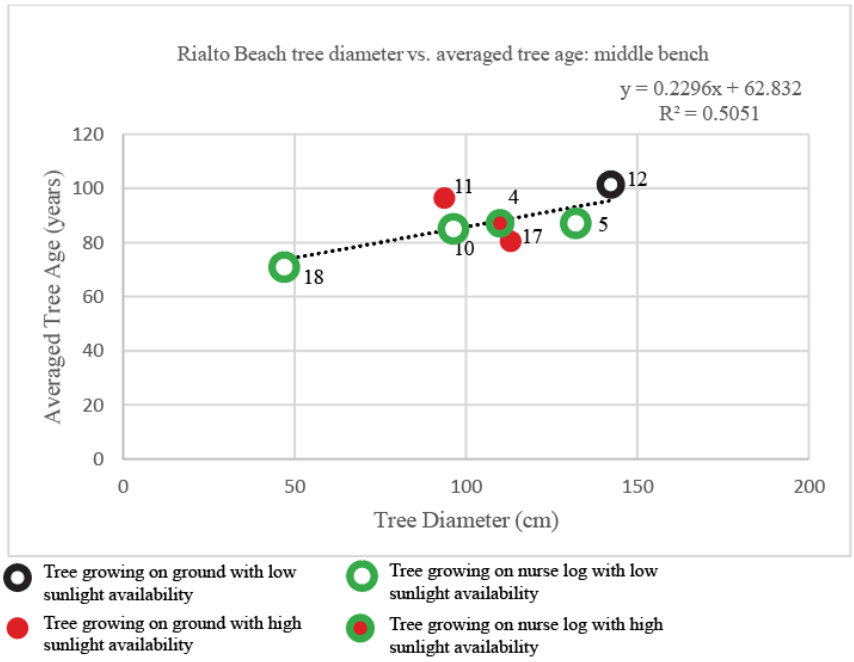

Figure 38. Graph of tree core diameter vs. averaged core age showing seven sampled trees from on or near the middle bench of LS1 (see Figure 23).

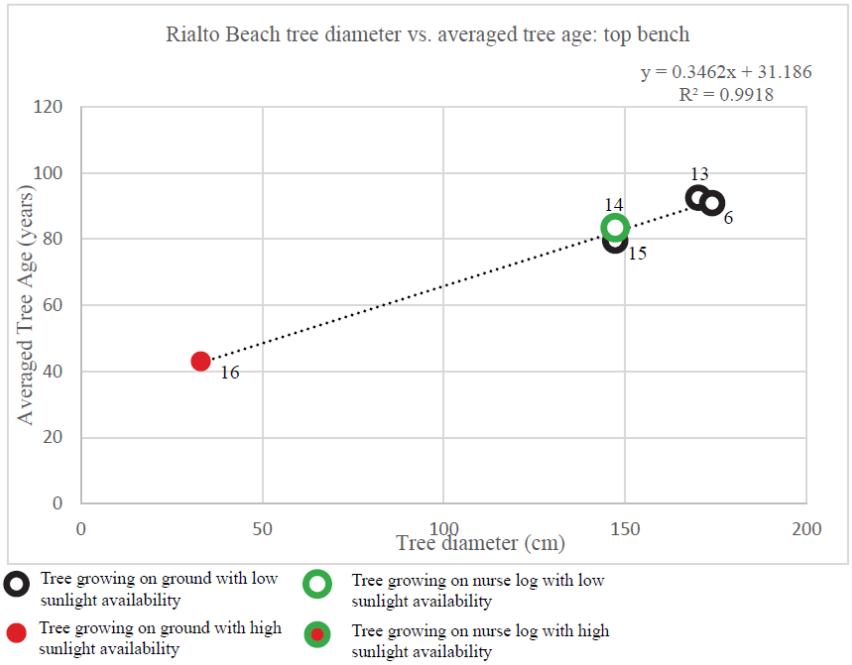

Figure 39. Graph of tree diameter vs. averaged core age showing five sampled trees from on or near the top bench of LS1 or above LS1 (see Figure 23).

Figure 40. Photo of a standing dead Sitka spruce located on the top bench of LS1. This and other standing dead trees may represent old forest that was killed during the Olympic Blowdown of 1921. Varqa Tavengar for scale.

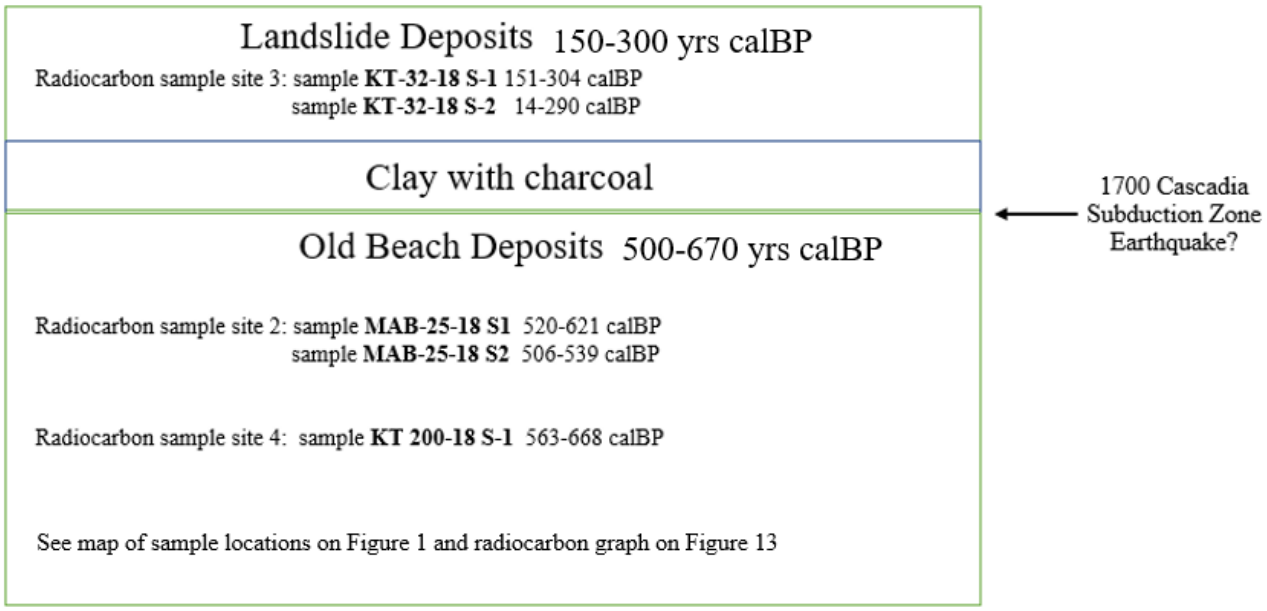

Figure 41. Shows stratigraphic section of the marine terrace exposure October 23, 2019, with units E (landslide deposit), unit G (clay with charcoal), unit C (old beach deposit) and unit B (old beach deposit) exposed. To the right is a table showing radiocarbon samples and date ranges and samples taken from within the respective units within the terrace.

Appendix Figure 1. Tree core survey data

Tree Number	ID	Diameter (in)	Diameter (cm)	Core Age 1	Core Age 2	Average	CBH (ft)	Lat	Long	easting	northing	Locality Description	Nurse Log (Y/N)	Sunlight Availability
1	TCSS1	26.4	67.056	72	81	76.5	6.9	47.92379	-124.63861	625929	971384		N	
2	TCSS2	45.5	115.57	85	76	90.5	11.9	47.92423	-124.63881	625890	971547	On steep slope, contact between horsetail patch and salaal	Y	N
	TCSS3	27.8	70.612				7.23	47.92423	-124.63881	625890	971547	50 ft NW of TCSS-2, downslope on flat ground in horsetail. Tree has secondary smaller tree attaced, next to clear waterfall. Discarded core due to rot, but counted minimum of 70 rings.		
3	TCSS4	19.2	48.768	97	95	96	5.05	47.92445	-124.63855	625957	971625	Tree ~ 10 ft S of TCSS3, located on nurselog approximately 6 ft. high, not attached to other trees or with other trees surrounding, high sunlight availablility.	Y	Y
4	TCSS5	43.3	109.982	86	88	87	11.35	47.92415	-124.63793	626103	971507	Tree located above third bench, closest bench to beach. Tree growing on nurse log ~5 feet high, has multiple lobes/shapes. Tree alone, not surrounded by others, exposed to sunlight through clearing towards NW.	Y	Y
5	TCSS6	52	132.08	88	86	87	13.6	47.92383	-124.63733	626243	971384	On second bench in salaal and ferm, on ~7 ft tall nurse log, oriented N-S. attached to 2 smaller trees to N and S which block some sunlight.	Y	N
	SS7(TCSS7)	73.3	186.182									Dead Sitka spruce, measured standing, broken fron top. larger than living trees, to compare to fallen nurse logs	N	Y
	SS8(TCSS8)	104.1	264.414									Dead Sitka spruce, ~50 feet high, broken at top, twisted exposed inner, bark has been eroded away. On very top of hillslope	N	Y
	Ss9(TCSS9)	61.1	155.194									Dead sitka spruce, some bark still present, top broken off. On top of hillslope	N	Y
	Ss10(TCSS10)													
	Ss11(TcSS11)	97	246.38									Living Sitka spruce, too large to core. On top bench, with ferns, young and old forest, Branches growing toward SW, thick branches, very old-looking compared to newer growth	N	Y
6	TCSS12	68.5	173.99	79	103	91		47.9243	-124.63326	627248	971501	Large SS on top bench, soil sandy silt with some gravel.	Y	N
	TCSS13	34.1	86.614				8.95							
7	TCSS14	34.4	87.376	74	79	76.5	8.81	47.92377	-124.63833	625996	971372	Bent slightly toward SE, on midslope of first bench on well-travelled path, near horsetail and skunk cabbage. Not surrounded by other trees, soil poorly drained.	N	Y

Tree Number	ID	Diameter (in)	Diameter (cm)	Core Age 1	Core Age 2	Average	CBH (ft)	Lat	Long	easting	northing	Locality Description	Nurse Log (Y/N)	Sunlight Availability
	TCSS15	/												
8	TCSS16	34.4	87.376	77	78	77.5		47.92407	-124.63918	625796	971494	On beach terrace, evidence of salt spray, in a line of other trees that appear to have grown on nurse logs. Soil appears to be colluvium material.	Y	Y
	TCSS17		0											
9	TCSS18	53	134.62	60	62	61						Located on first bench, in loamy soil. Ferns, oregon grape, not water-loving plants. Nurse log oriented N-S	Y	Y
10	TCSS19	38	96.52	89	81	85						On slope going up to second bench, on nurse log. Sun partially blocked by tree, nurse log oriented E-W.	N	Y
11	TCSS20	36.9	93.726	103	90	96.5						On nurse log 50 ft. from TCSS19, same elvation on bench slope.Sun blocked by neighboring trees.	Y	N
12	TCSS21	56	142.24	115	88	101.5						Partially obscured by other trees, very loamy soil, more open understory, straighter growth orientation of trees, lots of fern, huckleberry, oregon grape, elk sign. Less double-trunk trees.	N	N
	TCSS22												Y	N
13	TCSS23	67	170.18	98	87	85						On upper bench, mostly obscurbed from sunlight same location properties as TCSS-21	Y	N
14	TCSS24	58	147.32	84	81	96.5						Upper bench, partially obscured light, denser and more mature underbrush. On nurse log. Less ferns, more downed trees underfoot.	N	N
15	TCSS25	58	147.32	80	79	101.5						Same location description as TCSS23 but on elevated surface (larger nurse log or stump)	N	Y
16	TCSS26	13	33.02	40	46	43						Located on top bench.Collected samples as through-core. Tree mossy, root pistol-butts to northwest, spare underbrush, lots of fern. Limited light, few lower branches, no nurse log.	Y	N
17	TCSS27	44.5	113.03	79	82	80.5						Located on second bench. Lots of sunlight, not growing on nurse log. Thick underbrush of ferns and salaal.	Y	N
18	TCSS28	18.5	46.99	73	69	71						Growing on nurse stump on slope between top and middle bench. Low sunlight availability, trees surrounding in all directions.	Y	N
19	TCSS29	15.4	39.116	43	43	43						On slope between beach berm and first bench. Pistol-butted on nurse log, limited sun, thick fern, oregon grape, salaal underbrush. Collected as one through-core.	Y	Y

Appendix 2: OxCal graphs for radiocarbon samples from OxCal IntCal v.13, Reimer et al 2013

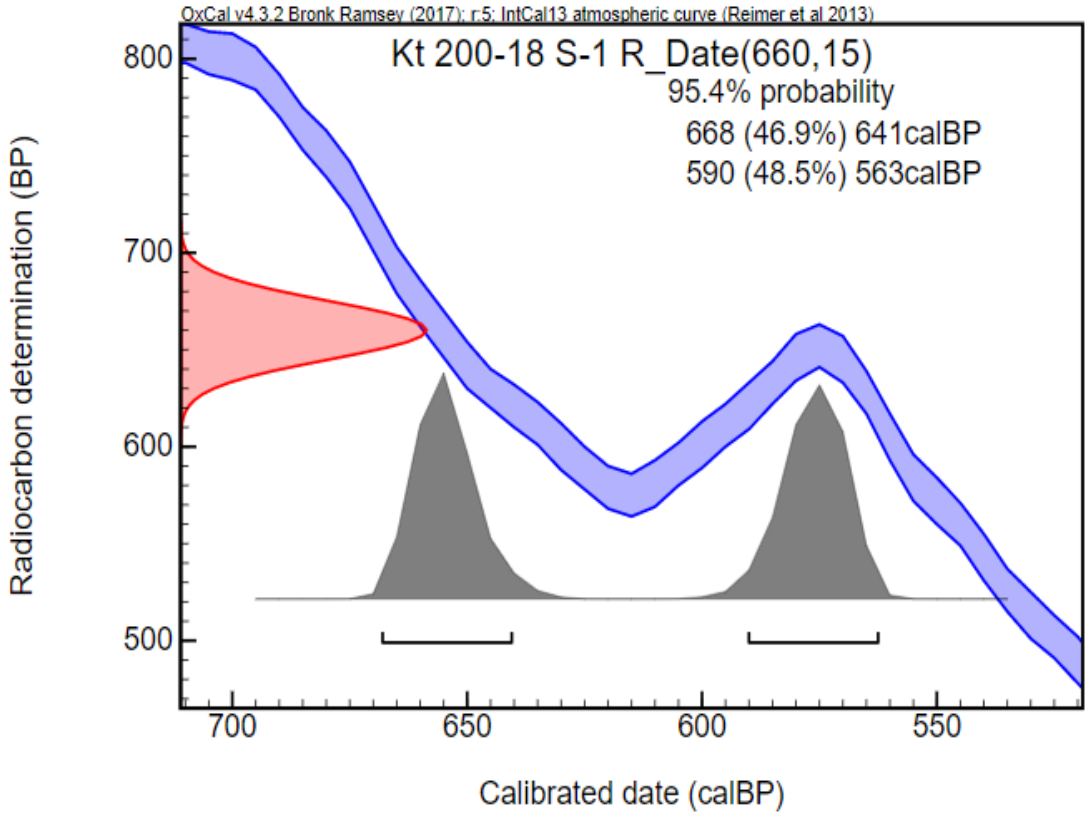

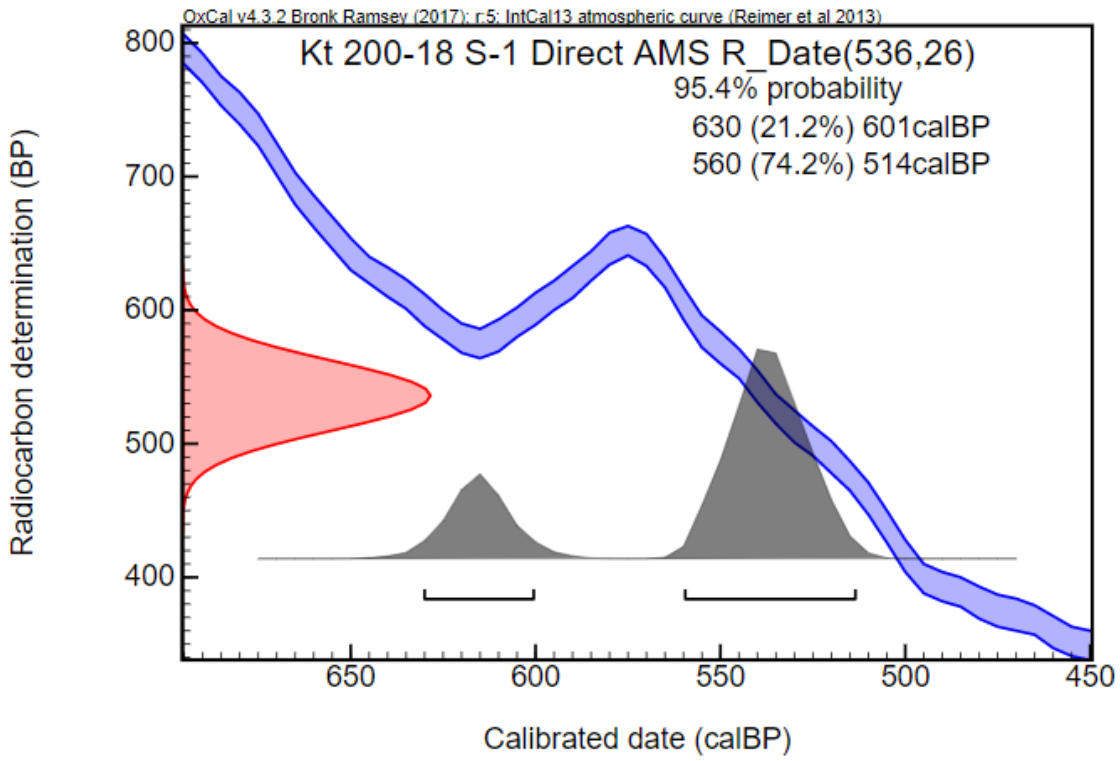
OxCal v4.3.2 Bronk Ramsey (2017); r:5; IntCal13 atmospheric curve (Reimer et al 2013)
Kt 200-18 S-1 Direct AMS R_Date(536,26)
95.4% probability
630 (21.2%) 601calBP
560 (74.2%) 514calBP
Radiocarbon determination (BP)
800
700
600
500
400
650
600
550
500
450
Calibrated date (calBP)

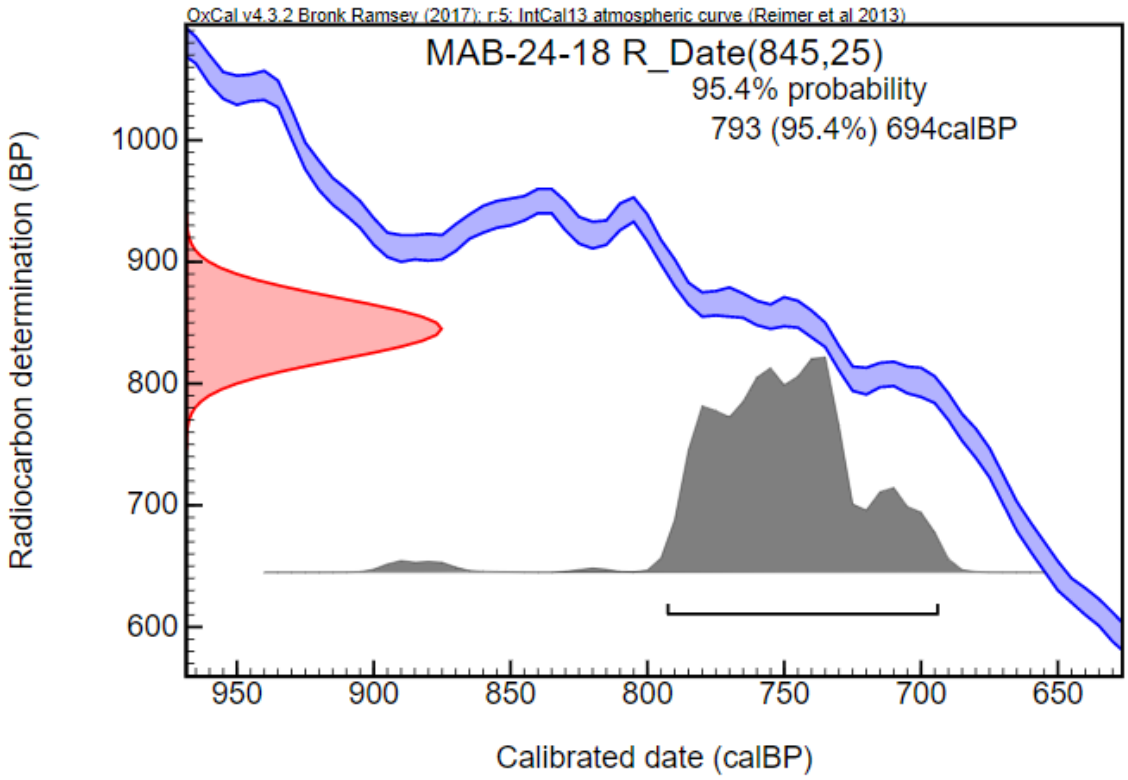
OxCal v4.3.2 Bronk Ramsey (2017); r:5; IntCal13 atmospheric curve (Reimer et al 2013)
MAB-24-18 R_Date(845,25)
95.4% probability
793 (95.4%) 694calBP
Radiocarbon determination (BP)
1000
900
800
700
600
950
900
850
800
750
700
650
Calibrated date (calBP)

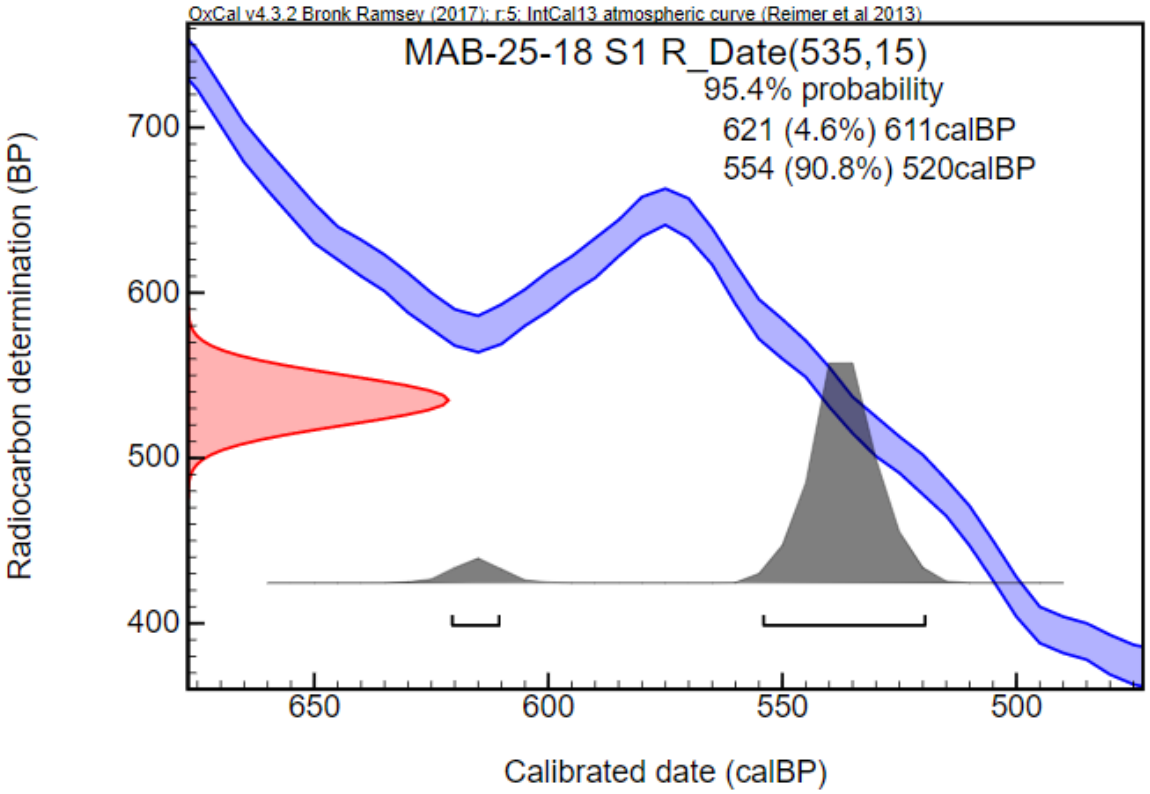
OxCal v4.3.2 Bronk Ramsey (2017); r:5; IntCal13 atmospheric curve (Reimer et al 2013)
MAB-25-18 S1 R_Date(535,15)
95.4% probability
621 (4.6%) 611calBP
554 (90.8%) 520calBP
Radiocarbon determination (BP)
700
600
500
400
650
600
550
500
Calibrated date (calBP)

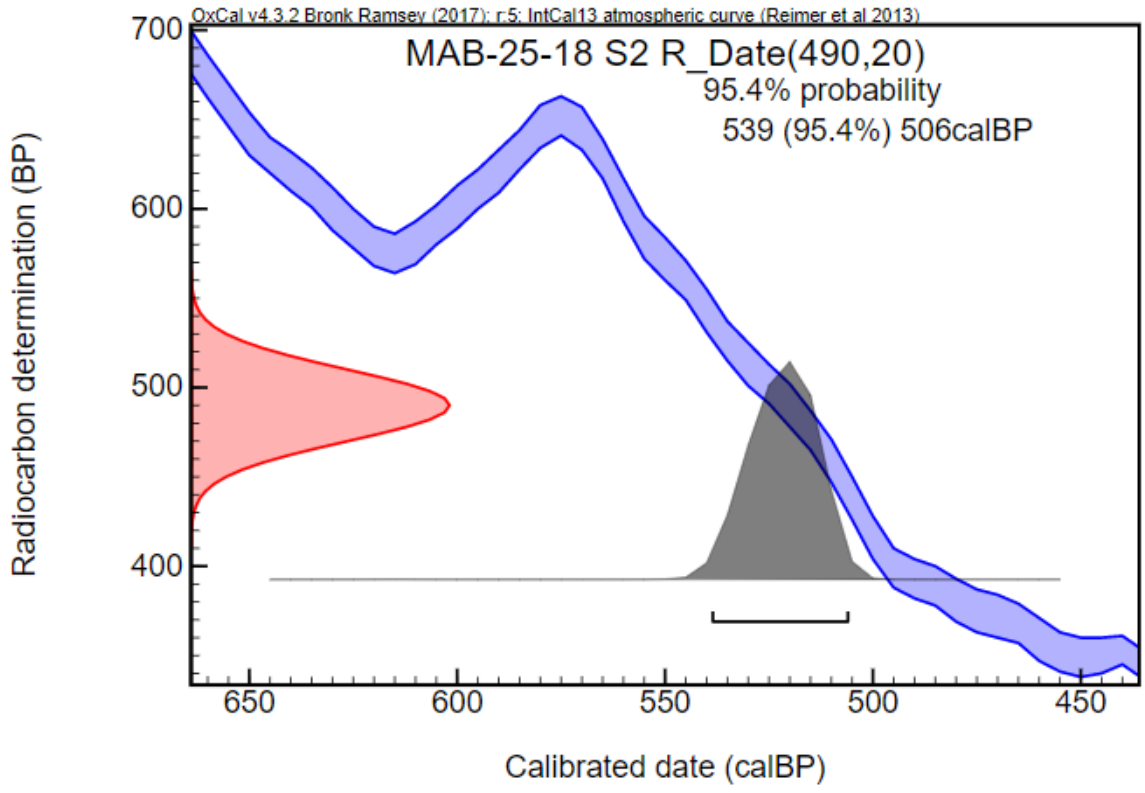
OxCal v4.3.2 Bronk Ramsey (2017); r:5; IntCal13 atmospheric curve (Reimer et al 2013)
MAB-25-18 S2 R_Date(490,20)
95.4% probability
539 (95.4%) 506calBP
Radiocarbon determination (BP)
700
600
500
400
650
600
550
500
450
Calibrated date (calBP)

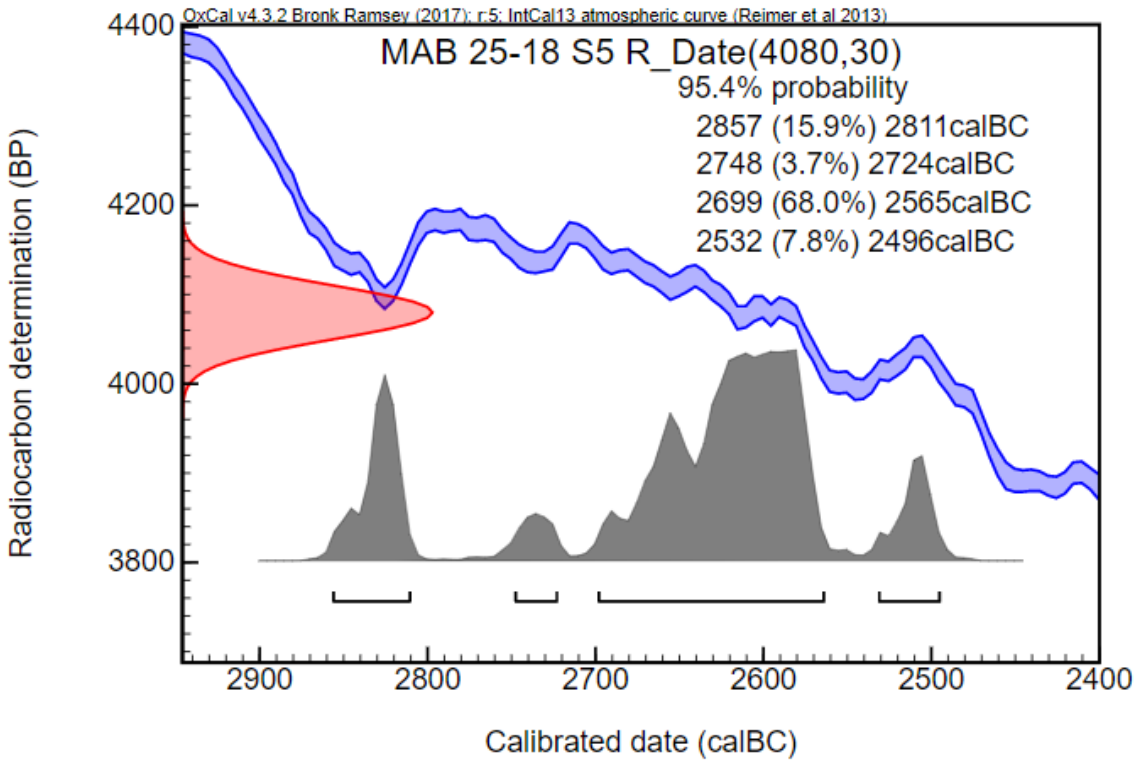
OxCal v4.3.2 Bronk Ramsey (2017); r:5; IntCal13 atmospheric curve (Reimer et al 2013)
MAB 25-18 S5 R_Date(4080,30)
95.4% probability
2857 (15.9%) 2811calBC
2748 (3.7%) 2724calBC
2699 (68.0%) 2565calBC
2532 (7.8%) 2496calBC
Radiocarbon determination (BP)
4400
4200
4000
3800
2900
2800
2700
2600
2500
2400
Calibrated date (calBC)

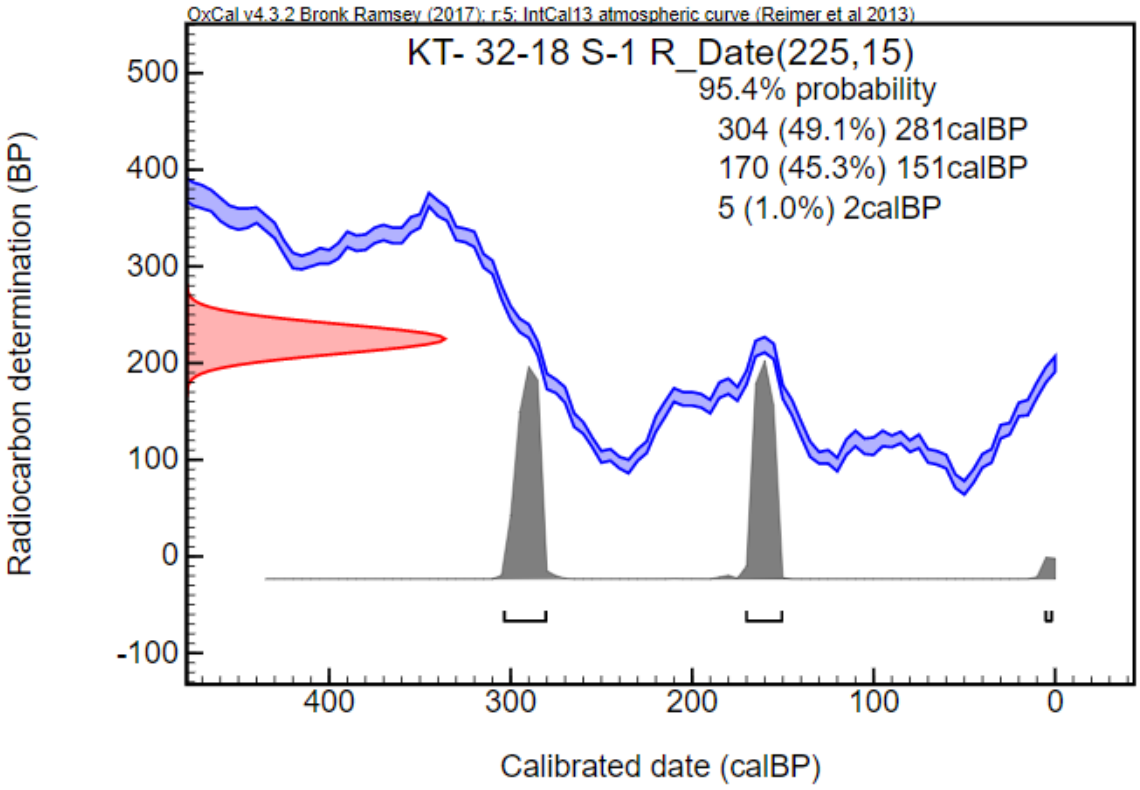
OxCal v4.3.2 Bronk Ramsey (2017); r:5; IntCal13 atmospheric curve (Reimer et al 2013)
KT- 32-18 S-1 R_Date(225,15)
95.4% probability
304 (49.1%) 281calBP
170 (45.3%) 151calBP
5 (1.0%) 2calBP
Radiocarbon determination (BP)
500
400
300
200
100
0
-100
400
300
200
100
0
Calibrated date (calBP)

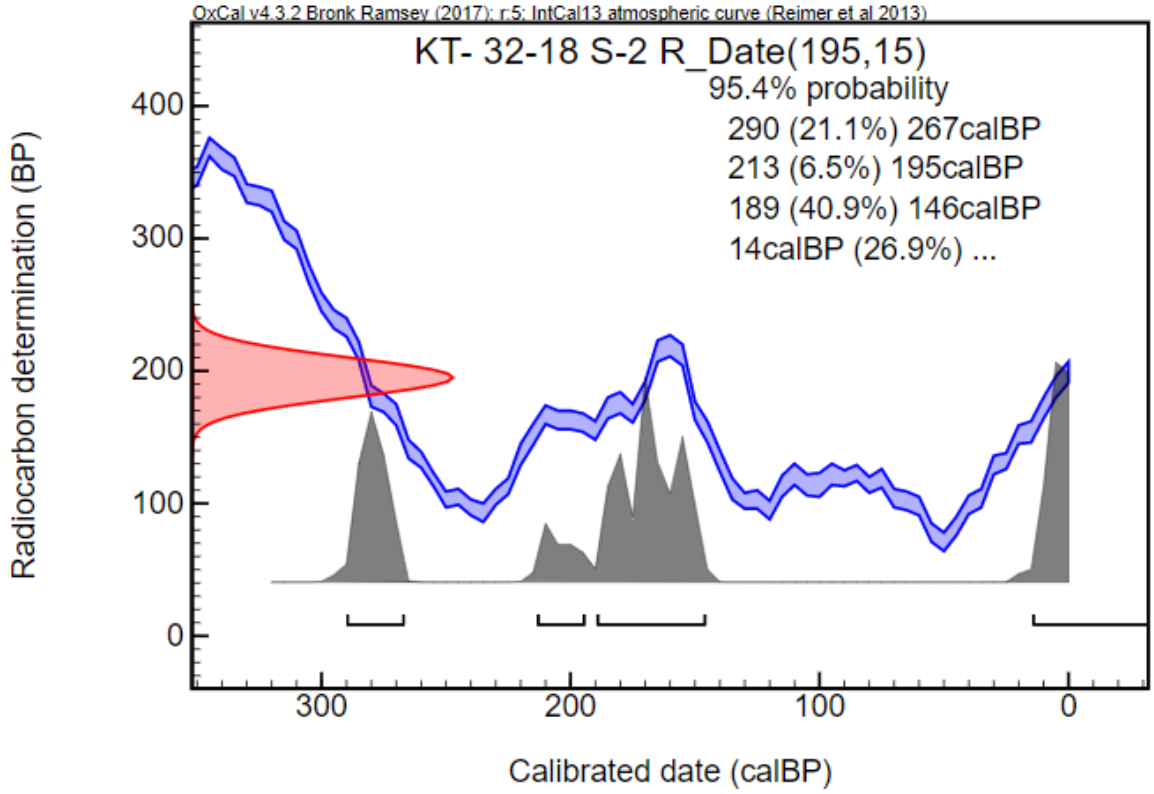
OxCal v4.3.2 Bronk Ramsey (2017); r:5; IntCal13 atmospheric curve (Reimer et al 2013)
KT- 32-18 S-2 R_Date(195,15)
95.4% probability
290 (21.1%) 267calBP
213 (6.5%) 195calBP
189 (40.9%) 146calBP
14calBP (26.9%) ...
Radiocarbon determination (BP)
400
300
200
100
0
300
200
100
0
Calibrated date (calBP)

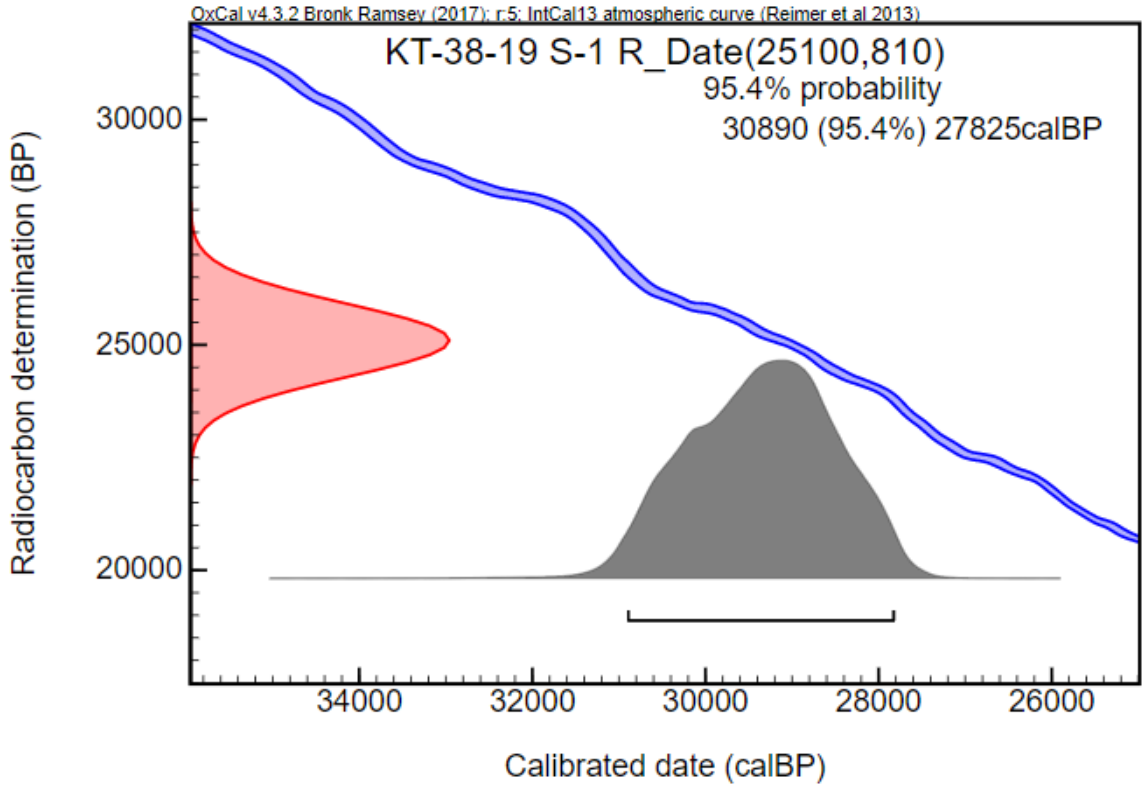
OxCal v4.3.2 Bronk Ramsey (2017); r:5; IntCal13 atmospheric curve (Reimer et al 2013)
KT-38-19 S-1 R_Date(25100,810)
95.4% probability
30890 (95.4%) 27825calBP
Radiocarbon determination (BP)
30000
25000
20000
34000
32000
30000
28000
26000
Calibrated date (calBP)